

## Solution and Structural Characterization of Iron(II) Complexes with *Ortho*-Halogenated Phenolates: Insights Into Potential Substrate Binding Modes in Hydroquinone Dioxygenases

Sara S. Rocks,<sup>†</sup> William W. Brennessel,<sup>†</sup> Timothy E. Machonkin,<sup>\*,‡</sup> and Patrick L. Holland<sup>\*,†</sup>

<sup>†</sup>Department of Chemistry, University of Rochester, Rochester, New York 14627, United States, and

<sup>‡</sup>Department of Chemistry, Whitman College, Walla Walla, Washington 99362, United States

Received July 10, 2010

The new ligand *cis,cis*-1,3,5-tris-(*E*)-(tolylideneimino)cyclohexane (TACH-*o*-tolyl) forms a 1:1 complex with iron(II). Addition of substituted phenolates forms 1:1:1 ligand:iron:phenolate complexes, which have been characterized both in the solid state and in solution. There is complete binding of the phenolate to the complex only when there are *ortho*-halogens on the phenolate. The tertiary complexes with *ortho*-halo-substituted phenolates exhibit short Fe–halogen distances, and the complex containing a non-coordinating but similarly sized *ortho*-methyl phenolate has a significantly different conformation and coordination geometry. Therefore, it is likely that the metal–halogen interaction stabilizes the complexes. The iron(II)–halogen interaction in these complexes may explain the substrate specificity of PcpA and LinE, enzymes that preferentially bind phenols and hydroquinones containing halogen substituents in *ortho* positions.

### Introduction

The remediation of chlorinated pollutants is an area of significant interest to the scientific community. Pentachlorophenol (PCP) is a carcinogen and a biocide that is still used in the United States; however, its use has been restricted since 1987 to use as a wood preservative for power poles and railroad ties.<sup>1</sup> The stability and attendant longevity of such chlorinated pollutants in the environment have created a problem that spans generations. One strategy for dealing with this problem is bioremediation, which requires the isolation of organisms that have evolved the capability to degrade undesirable molecules such as PCP. Some bacteria can degrade chlorophenols, but their tolerance of different chlorophenols is very specific to the degree of chlorination of the ring.<sup>2</sup> Interestingly, some bacteria, such as *Sphingobium chlorophenolicum* (formerly called *Sphingomonas chlorophenolica*) ATCC 39723, can use pentachlorophenol as their sole carbon source.<sup>3</sup>

The degradation pathway for pentachlorophenol by *S. chlorophenolicum* is shown in Scheme 1.<sup>4,5</sup> The key oxidative ring cleavage step is catalyzed by 2,6-dichlorohydroquinone 1,2-dioxygenase (PcpA), which is an iron(II) dependent enzyme.<sup>5,6</sup>  $\gamma$ -Hexachlorocyclohexane, or lindane, is also catabolized through a chlorohydroquinone cleavage pathway that includes the enzyme chlorohydroquinone 1,2-dioxygenase, LinE.<sup>7</sup> Thus, the PCP and lindane pathways proceed through the oxidative ring cleavage of a chlorinated hydroquinone catabolic intermediate. This is a key difference from most bacterial arene degradation pathways, which proceed through the oxidative ring cleavage of a catechol.<sup>8</sup> LinE and PcpA are both non-heme iron(II)-containing dioxygenases, like the well-studied extradiol catechol dioxygenase (EDO) enzymes.<sup>8</sup> Site-directed mutagenesis and homology modeling have determined that, like the EDOs, the iron(II) in PcpA is ligated facially by two histidines and a glutamate (Figure 1).<sup>9</sup> LinE has 51% sequence identity to PcpA, including the

\*To whom correspondence should be addressed. E-mail: machonte@whitman.edu (T.E.M.), holland@chem.rochester.edu (P.L.H.).

(1) (a) *Toxicological Profile for Pentachlorophenol*; PB/2001/109106/AS; U.S. Department of Health and Human Services, Agency for Toxic Substances and Disease Registry: Atlanta, GA, 2001. (b) *Reregistration Eligibility Decision for Pentachlorophenol*; EPA 739-R-08–008; U.S. Environmental Protection Agency, Office of Pesticide Programs: Arlington, VA, 2008.

(2) Hagblom, M. M. *FEMS Microbiol. Rev.* 1992, 103, 29–72.

(3) (a) Saber, D. L.; Crawford, R. L. *Appl. Environ. Microbiol.* 1985, 50, 1512–1518. (b) Ederer, M. M.; Crawford, R. L.; Herwig, R. P.; Orser, C. S. *Mol. Ecol.* 1997, 6, 39–49. (c) Nohynek, L. J.; Suhonen, E. L.; Nurmiaho-Lassila, E. L.; Hantula, J.; Salkinoja-Salonen, M. *Syst. Appl. Microbiol.* 1996, 18, 527–538.

(4) (a) Cai, M.; Xun, L. Y. *J. Bacteriol.* 2002, 184, 4672–4680. (b) Dai, M. H.; Copley, S. D. *Appl. Environ. Microbiol.* 2004, 70, 2391–2397.

(5) Xu, L.; Resing, K.; Lawson, S. L.; Babbitt, P. C.; Copley, S. D. *Biochemistry* 1999, 38, 7659–7669.

(6) (a) Ohtsubo, Y.; Miyauchi, K.; Kanda, K.; Hatta, T.; Kiyohara, H.; Senda, T.; Nagata, Y.; Mitsui, Y.; Takagi, M. *FEBS Lett.* 1999, 459, 395–398. (b) Xun, L.; Bohuslavsek, J.; Cai, M. *Biochem. Biophys. Res. Commun.* 1999, 266, 322–325.

(7) (a) Endo, R.; Kamakura, M.; Miyauchi, K.; Fukuda, M.; Ohtsubo, Y.; Tsuda, M.; Nagata, Y. *J. Bacteriol.* 2005, 187, 847–853. (b) Miyauchi, K.; Adachi, Y.; Nagata, Y.; Takagi, M. *J. Bacteriol.* 1999, 181, 6712–6719. (c) Nagata, Y.; Endo, R.; Ito, M.; Ohtsubo, Y.; Tsuda, M. *Appl. Microbiol. Biotechnol.* 2007, 76, 741–752.

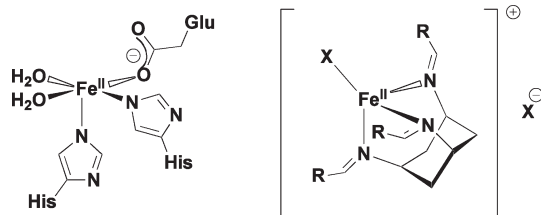
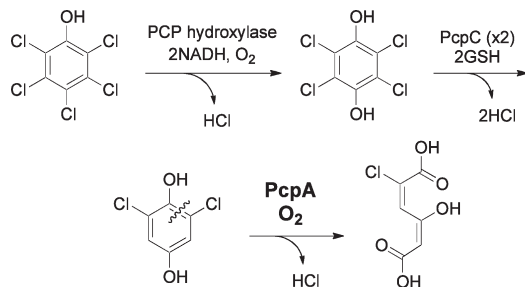


**Figure 1.** Proposed active site of PcpA based upon the resting state of EDOs (left) compared with the iron(II) complex of a TACH-based triimine ligand (right).

**Scheme 1.** Pathway for the Degradation of Pentachlorophenol in *S. chlorophenolicum*.<sup>4,5</sup>



conserved two histidines and glutamate, suggesting that it has a similar active site.<sup>7</sup>

Though EDO enzymes and the chlorohydroquinone dioxxygenase enzymes have similar activities (oxidative ring cleavage), metal ion cofactor (iron(II)), and active site ligands (two histidines, one glutamate), there is a surprising difference between the different types of enzymes. Namely, EDO enzymes are *inactivated* by chlorinated substrates,<sup>10</sup> while PcpA and LinE use chlorinated molecules as their *native* substrates.<sup>5–7</sup> It is interesting that iron(II) active sites with similar geometry that catalyze similar reactions have such different patterns of selectivity and inactivation. Understanding the differences between catechol dioxygenases and PcpA may help to elucidate the mechanisms through which specificity for chlorinated substrates can arise. This information, in turn, may help scientists to design and utilize better systems for bioremediation of chlorinated pollutants.

One way to explore the determinants of substrate selectivity is through the synthesis of model complexes with the same metal and geometry as the enzyme. By design, these complexes lack the protein scaffold. By removing the influence

of the protein, it is possible to understand the inherent selectivity, binding modes, and reactivity of the metal ion. Using this information, one may deconvolute the factors that stem from the inherent chemistry of the metal center from those that come from the protein active site pocket. For PcpA, such data are essential in the effort to develop an understanding of how this enzyme uses chlorinated substrates without inactivation.

Catechol complexes of iron have been studied for many years to provide insight into substrate binding, spectroscopy, and mechanism of EDO enzymes.<sup>11</sup> On the other hand, little synthetic chemistry has been done to elucidate the binding of hydroquinones (the substrates of PcpA and LinE) with mononuclear iron complexes. A search of the Cambridge Crystallographic Database (CCD) and Gmelin produced only one example of a chlorinated hydroquinone on iron, an unpublished structure of a diiron(III) porphyrin complex bridged by tetrachlorohydroquinonate.<sup>12</sup> This example highlights a significant difficulty, which is that hydroquinones can bridge multiple metal ions. In the only two known solid-state structures containing an unsupported hydroquinone coordinated to non-heme iron, the hydroquinone bridges between metals.<sup>13</sup>

In the work presented below, the strategy for avoiding hydroquinone bridging was to use phenols as proxies for hydroquinones, which assumes that the *para* hydroxyl group does not alter the influence of *ortho*-halogen substituents on phenolate binding. The idea that phenols bind similarly to hydroquinones in the enzyme is supported by the fact that *ortho*-halogenated phenols are potent inhibitors of PcpA.<sup>14</sup> Interestingly, even with the more common phenolate as a ligand, iron(II) coordination chemistry is understudied. Though many iron(III)-phenolate complexes are known, iron(II) complexes with unsupported phenolate ligands are comparatively rare (see Discussion below). The known iron-phenolate complexes do not provide insight into the influence of chlorine substituents on iron binding because there are no crystallographically characterized mononuclear complexes of iron(II) with chlorinated phenolates.<sup>15</sup>

The goal of this work was to investigate the fundamental coordination chemistry of non-tethered hydroquinones and phenols on a Fe(II) center supported by a tridentate ligand, and to examine how *ortho*-substituents affect the binding mode. These synthetic model compounds are expected to elucidate the possible origins of substrate selectivity in LinE and PcpA, and to expand our understanding of the basic coordination chemistry of *ortho*-halogenated phenols on iron(II).

## Results

**Ligand Design Strategy.** *cis,cis*-1,3,5-Triaminocyclohexane (TACH) is a well-precedented template for the synthesis of multidentate ligands that are preorganized to

(8) (a) Bugg, T. D. H.; Winfield, C. J. *Nat. Prod. Rep.* **1998**, 513–530. (b) Solomon, E. I.; Brunold, T. C.; Davis, M. I.; Kemsley, J. N.; Lee, S.-K.; Lehnert, N.; Neese, F.; Skulan, A. J.; Yang, Y.-S.; Zhou, J. *Chem. Rev.* **2000**, *100*, 235–349. (c) Bugg, T. D. H.; Lin, G. *Chem. Commun.* **2001**, 941–952. (d) Vaillancourt, F. H.; Bolin, J. T.; Eltis, L. Ring-Cleavage Dioxygenases. In *Pseudomonas*; Ramos, J.-L., Ed.; Kluwer Academic/Plenum: New York, 2004; Vol. 3, pp 359–396. (e) Vaillancourt, F. H.; Bolin, J. T.; Eltis, L. D. *Crit. Rev. Biochem. Mol. Biol.* **2006**, *41*, 241–267. (f) Bugg, T. D. H.; Ramaswamy, S. *Curr. Opin. Chem. Biol.* **2008**, *12*, 134–140.

(9) Machonkin, T. E.; Holland, P. L.; Smith, K. N.; Liberman, J. S.; Dinescu, A.; Cundari, T. R.; Rocks, S. S. *J. Biol. Inorg. Chem.* **2010**, *10*, 291–301.

(10) (a) Klecka, G. M.; Gibson, D. T. *Appl. Environ. Microbiol.* **1981**, *41*, 1159–1165. (b) Bartels, I.; Knackmuss, H.-J.; Reineke, W. *Appl. Environ. Microbiol.* **1984**, *47*, 500–505. (c) Cerdan, P.; Wasserfallen, A.; Rekik, M.; Timmis, K. N.; Harayama, S. *J. Bacteriol.* **1994**, *176*, 6074–6081. (d) Vaillancourt, F. H.; Labbé, G.; Drouin, N. M.; Fortin, P. D.; Eltis, L. D. *J. Biol. Chem.* **2002**, *277*, 2019–2027. (e) Dai, S.; Vaillancourt, F. H.; Maaroufi, H.; Drouin, N. M.; Neau, D. B.; Snieckus, V.; Bolin, J. T.; Eltis, L. D. *Nat. Struct. Biol.* **2002**, *9*, 934–939.

(11) Costas, M.; Mehn, M. P.; Jensen, M. P.; Que, L. *Chem. Rev.* **2004**, *104*, 939–986.

(12) Rheingold, A. L.; Miller, J. Private Communication to Cambridge Structural Database, **2003**.

(13) (a) Heistand, R. H.; Roe, A. L.; Que, L. *Inorg. Chem.* **1982**, *21*, 676–681. (b) Maroney, M. J.; Day, R. O.; Psyris, T.; Fleury, L. M.; Whitehead, J. P. *Inorg. Chem.* **1989**, *28*, 173–175.

(14) Doerner, A. E.; Machonkin, T. E. unpublished work.

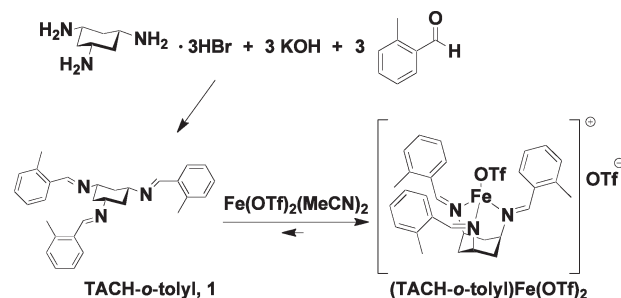
(15) Cambridge Structural Database, v. 5.31 (November 2009 update); Allen, F. H. *Acta Crystallogr.* **2002**, *B58*, 380–388.

give *fac* coordination of three donor atoms. In the work described here, we use imine donors because of the electronic similarity to the biological histidine residues. The ability to control the level of steric protection around the metal is an additional asset in this class of ligands, since TACH can be condensed with a variety of different aldehydes.<sup>16</sup> These factors made a TACH-based imine an attractive choice of ligand with which to synthesize a 1:1 ligand:iron(II) complex that would have additional coordination sites on iron for phenolate binding.

The reaction of *cis,cis*-1,3,5-tris-(*E*)-benzylideneaminocyclohexane (TACH-benz) with copper(II), zinc(II), and nickel(II) has been reported, and the use of hydrated metal salts led to partial hydrolysis of the ligand.<sup>17</sup> In the work presented here, rigorous exclusion of water during the reaction of Fe(II) with TACH-benz prevented ligand hydrolysis. Preliminary reactions of TACH-benz with iron(II) triflate in CD<sub>3</sub>CN (using techniques similar to those described below) indicated that addition of only one molar equivalent of ligand led to formation of a 2:1 ligand:iron(II) complex, and therefore the phenyl groups did not provide sufficient steric bulk.<sup>18</sup> A TACH-based ligand with mesityl groups instead of phenyl groups has been reported to form a 1:1 complex with Cu(II),<sup>19</sup> but when we treated an isosteric ligand containing 2,6-dimethylphenyl substituents (*cis,cis*-1,3,5-tris-(*E*)-xylylideneaminocyclohexane, TACH-xyl) with iron(II), <sup>1</sup>H NMR spectra indicated incomplete binding. We surmised that this ligand was too bulky to form the desired 1:1 complex of tridentate ligand and iron(II).<sup>18</sup>

Therefore, we prepared a new tridentate ligand with intermediate steric demands that would allow adequate binding of the metal ion while still precluding the formation of the bis-ligand complex. This compound, *cis,cis*-1,3,5-tris-(*E*)-(tolylideneimino)cyclohexane (TACH-*o*-tolyl, **1**), was prepared by condensation of TACH and *ortho*-tolualdehyde and isolated in 78% yield (Scheme 2). Compound **1** was combined with iron(II) triflate in CD<sub>3</sub>CN, and the resulting solution was analyzed by <sup>1</sup>H NMR spectroscopy. Nine signals are anticipated in complexes of **1**, assuming a C<sub>3</sub> axis of symmetry through the ligand. In the <sup>1</sup>H NMR spectrum of the solution, there are five highly shifted signals at  $\delta$  301, 268, 18.3, -3.5, and -12.6 ppm, and four signals are observed in the diamagnetic region (0–10 ppm) amid smaller signals for unbound ligand. The relative integrations of bound and unbound ligand in the <sup>1</sup>H NMR spectrum indicate that roughly 70% of the ligand is bound to iron. The wide chemical shift dispersion in the <sup>1</sup>H NMR spectrum of the complex indicates that the iron(II) has a high-spin

**Scheme 2.** Synthesis of TACH-*o*-tolyl and its Iron(II) Complex



electronic configuration. The number of acetonitrile solvent molecules bound to iron is unknown.

A second equivalent of TACH-*o*-tolyl was added to a 1:1 mixture of ligand and iron(II) triflate in CD<sub>3</sub>CN, and the changes in the <sup>1</sup>H NMR signal intensities were determined with a capillary integration standard of cobaltocene. The paramagnetically shifted <sup>1</sup>H NMR signals did not increase in intensity, the free ligand signals did increase in intensity, and no new signals were observed. From the absence of new signals and lack of increased intensity of observed paramagnetic signals, we conclude that a 2:1 complex does not form between **1** and iron(II) triflate in CH<sub>3</sub>CN. Therefore, using an *ortho*-methyl group on the benzylidene arm provides enough steric bulk to prevent 2:1 ligand:metal complexes, yet not so much steric hindrance that metal binding is prevented in CH<sub>3</sub>CN. Anaerobic electrospray mass spectra of a solution generated from **1** and iron(II) triflate contained a signal at *m/z* 640 that corresponds to [Fe(TACH-*o*-tolyl)(OTf)]<sup>+</sup> (Scheme 2) and is consistent with the formation of a 1:1 ligand:Fe<sup>2+</sup> complex. The <sup>19</sup>F NMR spectrum has a single broadened peak near the position of free triflate, suggesting that the triflate anions rapidly exchange on and off of the metal. On the basis of these measurements, we formulate this complex as (TACH-*o*-tolyl)Fe(OTf)<sub>2</sub>, with the triflate ions exchanging between outer-sphere and inner-sphere in solution. Since the complex partially dissociates the TACH-*o*-tolyl ligand in solution, it exists as a mixture and therefore was not fully characterized. This mixture was typically formed in situ for subsequent reactions with phenolates; as seen below, addition of certain phenolates or hydroquinonates led to complete coordination of the TACH-*o*-tolyl ligand.

**<sup>1</sup>H NMR Studies of Reactions of (TACH-*o*-tolyl)Fe(OTf)<sub>2</sub> with Hydroquinones and Phenols.** A variety of substituted phenols, as well as unsubstituted phenol and methylhydroquinone, were each deprotonated to form solutions of phenolate and hydroquinonate anions. (In the remainder of the paper, “phenolate” will refer to either a 1:1 mixture of phenol and triethylamine or a sodium phenolate. The choice of deprotonation protocol led to no apparent differences in the <sup>1</sup>H NMR signals of the resulting complexes.) When each phenolate and hydroquinonate was reacted with a mixture of iron(II) triflate and **1** in CD<sub>3</sub>CN, the resultant <sup>1</sup>H NMR spectrum was consistent with the formation of the desired 1:1:1 ligand:iron:phenolate or ligand:iron:hydroquinonate complex. The <sup>1</sup>H NMR spectra are shown in Figure 2. For complexes of some of the phenolates, the electrospray mass spectrum was collected under rigorously anaerobic conditions, and

(16) (a) Boxwell, C. J.; Bhalla, R.; Cronin, L.; Turner, S. S.; Walton, P. H. *J. Chem. Soc., Dalton Trans.* **1998**, 2449–2450. (b) Cronin, L.; Foxon, S. P.; Lusby, P. J.; Walton, P. H. *J. Biol. Inorg. Chem.* **2001**, 6, 367–377. (c) Naim, A. K.; Bhalla, R.; Foxon, S. P.; Liu, X. M.; Yellowlees, L. J.; Gilbert, B. C.; Walton, P. H. *J. Chem. Soc., Dalton Trans.* **2002**, 1253–1255. (d) Archibald, S. J.; Foxon, S. P.; Freeman, J. D.; Hobson, J. E.; Perutz, R. N.; Walton, P. H. *J. Chem. Soc., Dalton Trans.* **2002**, 2797–2799.

(17) (a) Greener, B.; Cronin, L.; Wilson, G. D.; Walton, P. H. *J. Chem. Soc., Dalton Trans.* **1996**, 401–403. (b) Greener, B.; Moore, M. H.; Walton, P. H. *Chem. Commun.* **1996**, 27–28. (c) Cronin, L.; Greener, B.; Foxon, S. P.; Heath, S. L.; Walton, P. H. *Inorg. Chem.* **1997**, 36, 2594–2600.

(18) Further details: Rocks, S. S. Ph.D. Thesis, University of Rochester, Rochester, New York, 2009.

(19) Cushion, M.; Ebrahimpour, P.; Haddow, M. F.; Hallett, A. J.; Mansell, S. M.; Orpen, A. G.; Wass, D. F. *Dalton Trans.* **2009**, 1632–1635.



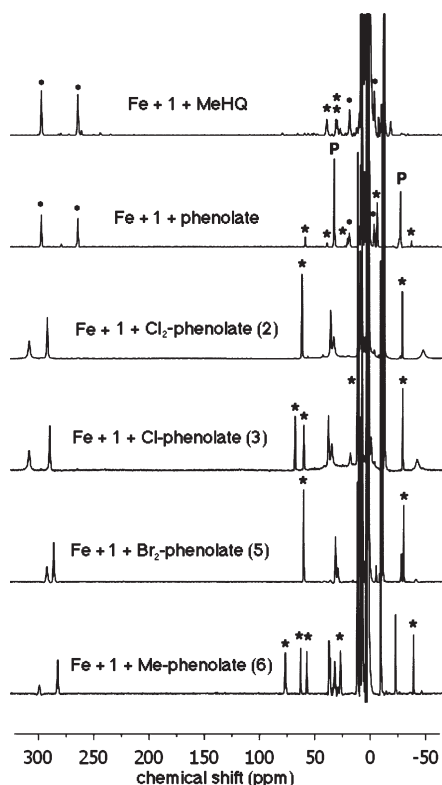


**Figure 2.**  $^1\text{H}$  NMR spectra of products from adding deprotonated 2-methylhydroquinone (MeHQ) or phenols to  $\text{Fe}(\text{OTf})_2 \cdot 2\text{CH}_3\text{CN}$  and **1** in  $\text{CD}_3\text{CN}$  at  $25^\circ\text{C}$ . Proton signals corresponding to the bound phenolates are denoted with an asterisk (\*). In the products from MeHQ and phenol, the peaks from  $(\text{TACH-}o\text{-tolyl})\text{Fe}(\text{OTf})_2$  (•) and “ $\text{Fe}(\text{phenolate})_n$ ” (P) are indicated, and the bound phenolate/hydroquinone peaks (\*\*) were assigned by deuterating the substrates.

these spectra showed a parent ion corresponding to the expected  $[(\text{TACH-}o\text{-tolyl})\text{Fe}(\text{phenolate})]^+$  cation (see Experimental Section). Crystal structures of some of the complexes (given in the next section) verify that the complexes are monomers in the solid state with a single  $\text{TACH-}o\text{-tolyl}$  ligand and a single phenolate coordinated to iron(II).

Mixing  $\text{Fe}(\text{OTf})_2 \cdot 2\text{CH}_3\text{CN}$ , **1**, and methylhydroquinone in  $\text{CH}_3\text{CN}$  resulted in a bright orange solution and a small amount of white precipitate. The  $^1\text{H}$  NMR spectrum showed the formation of a paramagnetic species with two highly shifted signals at  $\delta$  297 and 264 ppm and the remaining signals lying between  $\delta$  40 and  $-40$  ppm, as well as small amounts of unidentified impurities (Figure 2). The two signals at  $\delta$  297 and 264 ppm are tentatively assigned as the imine proton and the  $\alpha\text{-CH}$  of the cyclohexane ring, since these protons are closest to the paramagnetic iron(II) center and are therefore expected to experience the largest Fermi contact shift. A large signal at  $\delta$   $-12.5$  ppm, while overlapping with several smaller signals, integrates to approximately 9 protons and is assigned as the methyl protons of the tolyl groups. The signals corresponding to the hydroquinone ring protons were identified by performing the same reaction with methylhydroquinone- $d_3$  that was deuterated at the three ring positions. In the  $^1\text{H}$  NMR spectrum of the deuterated complex, signals at  $\delta$  29, 31, and 39 ppm were absent, showing that the corresponding resonances in the protonated analogue derive from the hydroquinonate ligand.

The remaining signals overlap to such an extent that further assignments are difficult. Even though they could not be fully assigned, the  $^1\text{H}$  NMR spectra indicate that a new species forms in the presence of 2-methylhydroquinonate, and from the integrations of non-overlapping signals, the observed species is consistent with the 1:1:1 iron(II): $\text{TACH-}o\text{-tolyl}$ :2-methylhydroquinonate complex. Unfortunately, this complex is unstable and decomposes to unidentified species at room temperature within hours, preventing further characterization.

Because of the instability of the hydroquinonate complex, subsequent reactions used phenolates, isosteric hydroquinone analogues that are likely to bind to iron(II) in PcpA because they are known inhibitors of enzymatic activity.<sup>14</sup> Mixing **1**,  $\text{Fe}(\text{OTf})_2 \cdot 2\text{CH}_3\text{CN}$ , and phenolate in  $\text{CD}_3\text{CN}$  yielded a bright yellow solution. Analysis by  $^1\text{H}$  NMR spectroscopy showed that binding of phenolate was incomplete (Figure 2). The highest intensity signals corresponded to  $(\text{TACH-}o\text{-tolyl})\text{Fe}(\text{OTf})_2$  and to a second species identified as “ $\text{Fe}(\text{phenolate})_n$ ”.<sup>20</sup> There was also a new species formed with an NMR signature that is consistent with the desired 1:1:1 complex. For the latter species, 11 signals were clearly observed while 12 are expected. Because of the congestion of the spectrum in the area from  $\delta$  11 to  $-3$  ppm, determining the exact number of signals that correspond to each product is difficult. Two signals at  $\delta$  279 and 265 ppm are assigned as the imine proton and the  $\alpha\text{-CH}$  of the cyclohexane ring, as above. Likewise, a large signal that integrates to 9 protons is observed at  $\delta$   $-12.3$  ppm and corresponds to the methyl groups of the tolylidene arms. Signals at  $\delta$  59, 39, and  $-37$  ppm that integrated to 2H, 2H, and 1H, respectively, were tentatively assigned as the *meta*, *ortho*, and *para* protons of the bound phenolate in the 1:1:1 complex. This assignment was confirmed by mixing  $\text{Fe}(\text{TACH-}o\text{-tolyl})(\text{OTf})_2$  with the deuterated phenolate  $\text{C}_6\text{D}_5\text{O}^-$  in  $\text{CD}_3\text{CN}$ , which gave a spectrum that was identical except for the absence of signals at these chemical shifts. Overall, the relative integrations and the approximate number of observed signals in the new species are consistent with formation of the desired 1:1:1 iron:ligand:phenolate product, although this is not the only species in solution.

To investigate the influence of *ortho*-substituents on binding, a variety of substituted phenolates were added to  $\text{Fe}(\text{TACH-}o\text{-tolyl})(\text{OTf})_2$ . Three different chlorinated phenols (2-chloro-, 2,6-dichloro-, and 2,3,4-trichlorophenol), 2,6-dibromophenol, and 2-methylphenol were each deprotonated with  $\text{Et}_3\text{N}$  and reacted with  $\text{Fe}(\text{OTf})_2$  and **1** in  $\text{CD}_3\text{CN}$ . The 2-methylphenolate complex behaved similarly to the parent phenolate, in that formation of the 1:1:1 complex was not complete. However, the  $^1\text{H}$  NMR spectra showed a single iron-containing product with each of the halogenated phenolates, consistent with complete binding of the phenolate and  $\text{TACH-}o\text{-tolyl}$  ligands. The significance of this important difference in binding will be discussed in more detail below.

The  $^1\text{H}$  NMR spectra of the complexes formed by reaction of  $\text{Fe}(\text{TACH-}o\text{-tolyl})(\text{OTf})_2$  with each of the

(20) The latter species was not characterized in detail, but was recognized from its presence in control reactions between  $\text{Fe}(\text{OTf})_2$  and phenolate without a supporting ligand. Additional spectra are shown in the Supporting Information.

substituted phenolates show very similar patterns of signals (Figure 2). The  $^1\text{H}$  NMR spectrum of each complex with a substituted phenolate shows two signals shifted downfield to between  $\delta$  289 and 313 ppm, which are assigned to the imine proton and  $\alpha$  CH of the cyclohexane ring. The signals from the methyl groups of the tolylidene arms integrate to 9H and are located between  $\delta$  -9 and -14 ppm in each case. The phenolate  $^1\text{H}$  NMR signals in each of the substituted phenolate complexes can be assigned by integration as well as by comparison between complexes with different substitution patterns. The signals corresponding to the TACH-*o*-tolyl ligand are at very similar chemical shifts in all five complexes, and the proton signals in the substituted phenolates are all at similar chemical shifts as those observed with the unsubstituted phenolate. In the 2-chlorophenolate complex (labeled **3** below), the *meta* protons are at  $\delta$  68 and 60 ppm, the *ortho* proton at 12 ppm, and the *para* proton at -30 ppm. In the 2,6-dichlorophenolate complex (labeled **2** below), the *meta* and *para* protons are at  $\delta$  62 and -29 ppm, and in the 2,6-dibromophenolate complex (labeled **5** below), the *meta* and *para* protons are at  $\delta$  60 and -30 ppm. In the 2-methylphenolate complex (labeled **6** below), the *meta* protons are at  $\delta$  63 and 57 ppm, the *ortho* proton at 26 ppm, the *para* proton at -39 ppm, and the methyl protons lie at  $\delta$  77 ppm. In the analogous 2,3,4-trichlorophenolate complex (which was characterized by  $^1\text{H}$  NMR spectroscopy only; see Supporting Information), the *meta* and *ortho* protons are at  $\delta$  60 and -2 ppm, respectively.

In all of these complexes, the signals with the largest downfield shifts (264–313 ppm) are assigned to the imine proton and the  $\alpha$  CH of the cyclohexane ring. Hyperfine shifts of this magnitude have been observed for the  $\text{RHC}=\text{N}-\text{CR}_2\text{H}$  moiety in mononuclear high-spin iron(II) complexes with imine ligands, and were ascribed to significant delocalization of unpaired spin density onto the imine. The  $-\text{CR}_2\text{H}$  proton has been observed at 195 ppm at 23 °C in a four-coordinate complex,<sup>21</sup> and the imine proton was observed at 460 ppm at 55 °C in a six-coordinate iron(II) complex.<sup>22</sup> In a ligand with a six-membered  $\pi$  system, such as a phenolate, the usual pattern is to be observed alternating upfield and downfield shifts of the ring protons, because of the alternating sign of the unpaired spin density.<sup>23</sup> In these phenolate complexes, this pattern is observed for the *meta* and *para* protons, which are observed at 59 to 68 and -29 to -39 ppm, respectively, but not for the *ortho* protons, which are observed at 39 to -2 ppm. This is probably due to a pseudocontact shift. A significant pseudocontact shift is expected for high-spin iron(II) systems,<sup>23</sup> especially for the phenolate *ortho* protons, which are close to the iron(II) center. Modest differences in the distance and the orientation with respect to the magnetic susceptibility tensor can lead to large variations in the pseudocontact shift, which could explain the large variation in the observed chemical shifts of the *ortho* protons in these complexes.

Several notable conclusions can be drawn from these  $^1\text{H}$  NMR studies. First, the solution-generated  $\text{Fe}(\text{TACH-}o\text{-tolyl})(\text{OTf})_2$  species binds a variety of phenols as well as methylhydroquinone. The adducts give similar  $^1\text{H}$  NMR spectra in each case. Second, each of the three *ortho*-halogenated phenols *completely* forms the 1:1:1 complex in solution, while the unsubstituted phenol, 2-methylphenol, and methylhydroquinone give incomplete binding. This observation suggests stronger binding affinity of the halogenated phenolate ligands to the TACH-*o*-tolyl-iron(II) complex. Third, the  $^1\text{H}$  NMR spectra indicate that the TACH-*o*-tolyl ligand in each of these complexes has  $C_3$  symmetry in solution on the NMR time scale, and the equivalence of the *meta* protons in the unsubstituted phenolate, the 2,6-dichlorophenolate, and 2,6-dibromophenolate complexes indicates fast rotation about the Fe–O and O–C bonds on the  $^1\text{H}$  NMR time scale (this issue will be revisited below).

**X-ray Crystallographic Studies of (TACH-*o*-tolyl)Fe(phenolate) Complexes.** The complexes were difficult to crystallize, which often prevented the acquisition of accurate microanalytical data for solids (the carbon analysis was often about 1% low, possibly from co-crystallization with salts). Despite the potential presence of impurities in the bulk sample, single crystals of a number of complexes were obtained and analyzed by X-ray diffraction.

Crystals of  $[\text{Fe}(\text{TACH-}o\text{-tolyl})(2,6\text{-dichlorophenolate})]\text{-OTf}$  (**2**) were obtained by two different methods. The first method used sodium 2,6-dichlorophenolate, concentration of the sample in hot tetrahydrofuran (THF) and slow diffusion of pentane vapor at -35 °C for two months. The second method used 2,6-dichlorophenol deprotonated with triethylamine, concentration of a THF solution at room temperature, and slow diffusion of  $\text{Et}_2\text{O}$  vapor at -35 °C for two months. While both methods produced single crystals of **2**, the crystals had different space groups ( $P2_1/c$  from the method with no heat and  $P2_12_12_1$  from the heated method). The  $P2_1/c$  structure had an asymmetric unit containing a single cation/anion pair while the asymmetric unit of the other structure ( $P2_12_12_1$ ) contained two discrete cation/anion pairs. Thus, there are three unique structures that provide information on bond lengths and angles for  $[\text{Fe}(\text{TACH-}o\text{-tolyl})(2,6\text{-dichlorophenolate})]\text{OTf}$ , Table 1, labeled **2A**, **2B**, and **2C** where **2A** is from the  $P2_1/c$  structure and **2B** and **2C** are from the  $P2_12_12_1$  structure. An ORTEP diagram of molecule **2B** is shown in Figure 3.

Two different methods were also used to crystallize the 2-chlorophenolate complex. In the first method, a mixture of **1**,  $\text{Fe}(\text{OTf})_2 \cdot 2\text{CH}_3\text{CN}$  and 2-chlorophenol deprotonated with triethylamine was stirred in THF for 15 min and then  $\text{Et}_2\text{O}$  vapor was diffused into the solution at -35 °C over the course of two weeks. Small yellow needles of  $[\text{Fe}(\text{TACH-}o\text{-tolyl})(2\text{-chlorophenolate})]\text{OTf}$  (**3**) formed. The crystals diffracted well, and the refined structure showed no solvent molecules in the unit cell. The molecule is disordered over two positions with the ligand tolylidene arms arranged in two orientations (1:1 ratio). In both conformers, the chloride of the phenolate is pointed toward the iron(II). An ORTEP diagram of the major conformer is shown in Figure 4. Bond lengths and angles of interest are listed in Table 2.

In the second crystallization method, a yellow solution in THF/ $\text{Et}_2\text{O}$  generated from iron(II) triflate, **1**, and

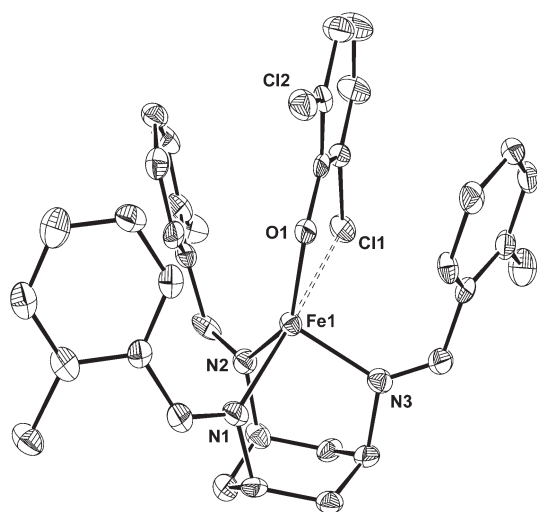
(21) Torzilli, M. A.; Colquhoun, S.; Kim, J.; Beer, R. H. *Polyhedron* **2002**, *21*, 705–713.

(22) Weber, B.; Walker, F. A. *Inorg. Chem.* **2007**, *46*, 6794–6803.

(23) Bertini, I.; Luchinat, C.; Parigi, G. *Solution NMR of Paramagnetic Molecules*; Elsevier: Amsterdam, 2001.

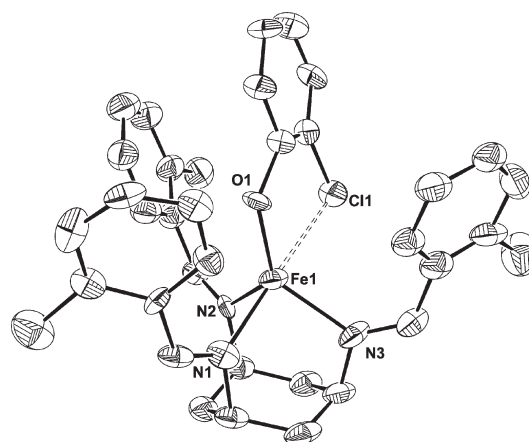
**Table 1.** Relevant Bond Lengths and Angles from the X-ray Structures of [Fe(TACH-*o*-tolyl)(2,6-dichlorophenolate)]OTf (**2**)

A		B		C	
Bond Lengths (Å)					
Fe1—O1	1.865(3)	Fe1—O1	1.885(3)	Fe2—O2	1.879(3)
Fe1—N3	2.061(5)	Fe1—N3	2.086(4)	Fe2—N6	2.084(4)
Fe1—N1	2.132(4)	Fe1—N1	2.143(4)	Fe2—N4	2.135(4)
Fe1—N2	2.070(5)	Fe1—N2	2.074(4)	Fe2—N5	2.078(5)
Fe1—Cl1	3.1224(17)	Fe1—Cl1	2.8898(15)	Fe2—Cl3	2.9877(16)
Bond Angles (deg)					
Fe1—O1—C31 <sub>phen</sub>	140.1(3)	Fe1—O1—C31	131.8(3)	Fe2—O2—C67	137.3(4)
N3—Fe1—N1	88.44(16)	N3—Fe1—N1	97.13(16)	N6—Fe2—N4	86.21(16)
N2—Fe1—N1	92.66(16)	N2—Fe1—N1	83.49(16)	N5—Fe2—N4	95.38(17)
N3—Fe1—N2	97.81(17)	N3—Fe1—N2	97.45(17)	N6—Fe2—N5	97.55(18)
O1—Fe1—N3	130.76(16)	O1—Fe1—N3	110.67(15)	O2—Fe2—N6	138.84(16)
O1—Fe1—N1	127.84(16)	O1—Fe1—N1	119.67(15)	O2—Fe2—N4	119.96(16)
O1—Fe1—N2	110.40(17)	O1—Fe1—N2	139.40(16)	O2—Fe2—N5	109.65(17)
N1—Fe1—Cl1	164.28(12)	N1—Fe1—Cl1	163.88(11)	N4—Fe2—Cl3	167.05(12)

**Figure 3.** One of three independent molecules in the solid state structure of [Fe(TACH-*o*-tolyl)(2,6-dichlorophenolate)]OTf, labeled molecule **2B**, with ellipsoids shown at 50% probability. Hydrogen atoms and the triflate anion are omitted for clarity.

2-chlorophenol deprotonated with triethylamine was concentrated by heating, and then stored at  $-35\text{ }^{\circ}\text{C}$  for 10 days to yield yellow blocks. Surprisingly, the crystals were not of the expected product, **3**, but were instead of [Fe(*cis*-TACH-*o*-tolyl)(2-chlorophenolate)(THF)]OTf (**4**) (Figure 5). In the *cis*-TACH-*o*-tolyl ligand, one imine C=N bond has isomerized to the *cis* stereoisomer, and thus it differs from the all-*trans* geometry observed in **2** and **3**. Also, unlike the structures of **2** and **3**, here the iron has an additional ligand: a THF molecule bound between the two *trans* tolylidene arms. The 2-chlorophenolate is disordered over two positions, where 91% of the time the chlorine is pointed outside the pocket and away from the metal and 9% of the time the chlorine is turned inside the binding pocket and toward the metal. Bond lengths and angles of interest are listed in Table 3.

It was also possible to grow crystals of the 2,6-dibromophenolate complex (**5**) by vapor diffusion of diethyl ether into a dimethoxyethane solution. The refined structure is shown in Figure 6, and distances and angles are in Table 4. As in the above structure, one arm of the TACH-*o*-tolyl ligand has isomerized. However, the space that is created

**Figure 4.** Solid state structure of conformer A of [Fe(TACH-*o*-tolyl)(2-chlorophenolate)]OTf (**3**) with ellipsoids shown at 50% probability. Hydrogen atoms and triflate anions are omitted for clarity.**Table 2.** Relevant Bond Lengths and Angles from the X-ray Structure of [Fe(TACH-*o*-tolyl)(2-chlorophenolate)]OTf (**3**)

	conformer A	conformer B
Bond Lengths (Å)		
Fe–O1/Fe'–O1'	1.915(7)	1.914(7)
Fe–N2/Fe'–N2'	2.097(5)	2.098(5)
Fe–N3/Fe'–N3'	2.100(5)	2.096(5)
Fe–N1/Fe'–N1'	2.101(5)	2.103(5)
Fe–Cl1/Fe'–Cl1'	2.929(7)	3.010(8)
Bond Angles (deg)		
Fe–O1–C31 <sub>phen</sub> /Fe'–O1'–C31' <sub>phen</sub>	120.7(13)	118.6(12)
N3–Fe–N2/N3'–Fe'–N2'	97.5(5)	97.3(5)
N3–Fe–N1/N3'–Fe'–N1'	91.0(4)	83.1(5)
N2–Fe–N1/N2'–Fe'–N1'	83.8(5)	91.0(4)
O1–Fe–N2/O1'–Fe'–N2'	124.7(8)	128.5(8)
O1–Fe–N3/O1'–Fe'–N3'	133.6(8)	127.8(8)
O1–Fe–N1/O1'–Fe'–N1'	110.0(7)	115.1(8)
N1–Fe–Cl1/N1'–Fe'–Cl1'	168.5(5)	163.4(5)

around the iron atom is filled not with a solvent molecule, but with one of the two bromo substituents of the phenolate with an iron–bromine bond distance of 2.8414(3) Å.

Combining **1** with iron(II) triflate and 2-methylphenolate resulted in an orange solution. Crystals of [Fe(TACH-*o*-tolyl)(2-methylphenolate)]OTf (**6**) were obtained



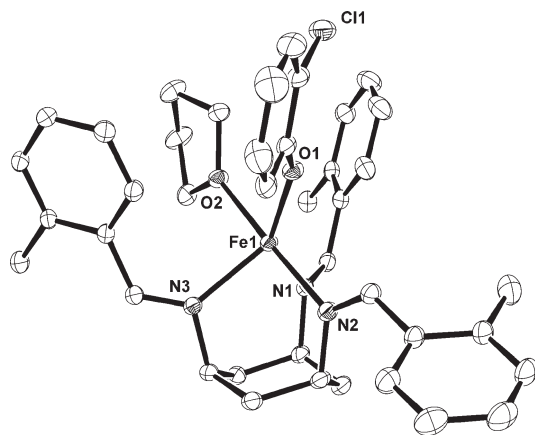


**Figure 5.** Solid state structure of the major conformer of  $[\text{Fe}(\text{cis-TACH-}o\text{-tolyl})(2\text{-chlorophenolate})(\text{THF})]\text{OTf}$  (**4**) with ellipsoids shown at 50% probability. Hydrogen atoms and triflate anion are omitted for clarity.

**Table 3.** Relevant Bond Lengths and Bond Distances for  $[\text{Fe}(\text{cis-TACH-}o\text{-tolyl})(2\text{-chlorophenolate})(\text{THF})]\text{OTf}$  (**4**) and for  $[\text{Fe}(\text{cis-TACH-}o\text{-tolyl})(\text{phenolate})(\text{THF})]\text{OTf}$  (**7**)

	4	7
Bond Lengths (Å)		
Fe1–O1	1.9202(9)	1.891(2)
Fe1–N1	2.1414(10)	2.148(2)
Fe1–N2	2.1758(10)	2.179(2)
Fe1–N3	2.1296(10)	2.119(2)
Fe1–O2	2.2007(8)	2.231(2)
Bond Angles (deg)		
N1–Fe1–N2	83.16(4)	86.56(9)
N2–Fe1–N3	91.08(4)	89.07(9)
N3–Fe1–N1	92.28(4)	93.60(9)
O1–Fe1–N1	135.49(7)	128.22(10)
O1–Fe1–N2	94.03(6)	96.91(9)
O1–Fe1–N3	132.22(7)	137.92(10)
O2–Fe1–O1	88.11(6)	87.51(8)
Fe1–O1–C31	139.99(18)	156.7(2)
O2–Fe1–N2	174.73(4)	174.74(8)

from vapor diffusion of  $\text{Et}_2\text{O}$  into a concentrated solution of **6** in dimethoxyethane over three weeks at  $-35^\circ\text{C}$ . The refined structure is shown in Figure 7, and relevant bond angles and distances are listed in Table 5. The iron atom in this structure is pseudotetrahedral with only four bonds. In contrast to the halogenated phenolates, the methyl group points away from the metal, in a less sterically crowded environment.

A concentrated yellow solution of **1**, iron(II) triflate, and phenolate in THF/ $\text{Et}_2\text{O}$  was heated, then stored at  $-35^\circ\text{C}$  for three days to yield yellow blocks. Similar to the case of the 2-chlorophenolate complex that was prepared from a hot THF/ $\text{Et}_2\text{O}$  solution, the crystals were not of the expected  $[\text{Fe}(\text{TACH-}o\text{-tolyl})(\text{phenolate})]\text{OTf}$  complex, but instead were  $[\text{Fe}(\text{cis-TACH-}o\text{-tolyl})(\text{phenolate})(\text{THF})]\text{OTf}$  (**7**) (Figure 8; metrical parameters in Table 3). Once again, one imine  $\text{C}=\text{N}$  bond in the TACH-*o*-tolyl has isomerized to the *cis* stereochemistry, and a THF molecule is ligated to the iron atom.

**Solution Ligand Dynamics and Isomerization.** The  $^1\text{H}$  NMR studies by themselves cannot definitively assign the nuclearity of these complexes in solution; however, the crystal structures indicate that they are monomers in the solid state. Although a monomer–dimer equilibrium in

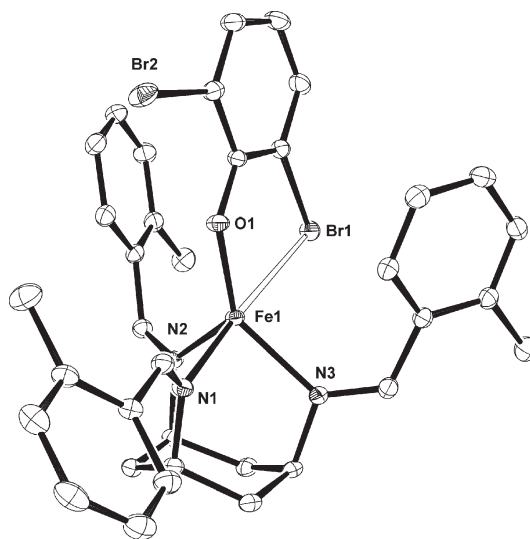


**Figure 6.** Solid state structure of  $[\text{Fe}(\text{cis-TACH-}o\text{-tolyl})(2,6\text{-dibromophenolate})]\text{OTf}$  (**5**) with ellipsoids shown at 50% probability. Hydrogen atoms and triflate anion are omitted for clarity.

**Table 4.** Relevant Bond Lengths and Bond Distances for  $[\text{Fe}(\text{cis-TACH-}o\text{-tolyl})(2,6\text{-dibromophenolate})(\text{THF})]\text{OTf}$  (**5**)

	5
Bond Lengths (Å)	
Fe1–O1	1.894(1)
Fe1–N3	2.100(1)
Fe1–N1	2.117(1)
Fe1–N2	2.079(1)
Fe1–Br1	2.8414(3)
Bond Angles (deg)	
Fe1–O1–C31 <sub>phen</sub>	130.80(9)
N3–Fe1–N1	86.43(5)
N2–Fe1–N1	91.80(5)
N3–Fe1–N2	97.29(5)
O1–Fe1–N3	137.97(5)
O1–Fe1–N1	100.29(5)
O1–Fe1–N2	123.60(5)
N1–Fe1–Br1	174.99(3)

solution is possible, the conditions for crystallization (high concentration, low temperature) favor dimer formation, while the crystal structures exclusively show mononuclear complexes. Also, electrospray mass spectra of selected complexes showed the presence of monomers. Therefore, for the remainder of the paper we describe the complexes in the context of a monomeric formulation.

The crystal structures of **2** show approximate  $C_s$  symmetry, with two of the tolylidene arms in similar orientations having the 2,6-dichlorophenolate sandwiched between them, and the third tolylidene arm in a very different orientation. Furthermore, in the crystal structures of **2** the *meta* protons of the phenolate are inequivalent. However, the room-temperature  $^1\text{H}$  NMR spectrum of **2** shows that the TACH-*o*-tolyl ligand has  $C_3$  symmetry on the NMR time scale, and the equivalence of the two *meta* protons on the phenolate indicates fast rotation of the phenolate on the NMR time scale. When the solution of **2** was cooled to  $-40^\circ\text{C}$ , two of the TACH-*o*-tolyl signals between  $\delta$  30 and 40 ppm split into two peaks each (Figure 9).

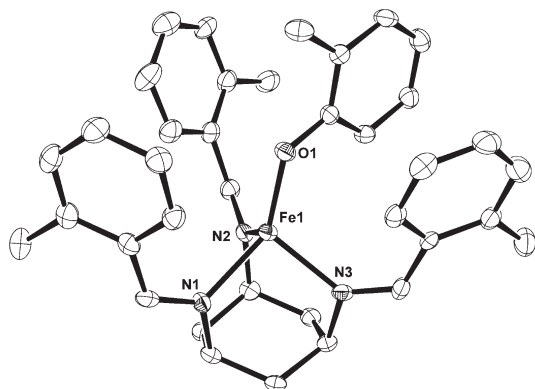


**Figure 7.** Solid state structure of [Fe(TACH-*o*-tolyl)(2-methylphenolate)]OTf (**6**) with ellipsoids shown at 50% probability. Hydrogen atoms and triflate anions are omitted for clarity.

**Table 5.** Relevant Bond Angles and Bond Lengths for [Fe(TACH-*o*-tolyl)(2-methylphenolate)] OTf (**6**)

6	
Bond Lengths (Å)	
Fe–O1	1.858(3)
Fe–N2	2.094(3)
Fe–N3	2.078(3)
Fe–N1	2.075(3)
Bond Angles (deg)	
Fe–O1–C31 <sub>phen</sub>	125.6(2)
N3–Fe–N2	95.73(12)
N3–Fe–N1	94.15(12)
N2–Fe–N1	87.08(12)
O1–Fe–N2	112.30(12)
O1–Fe–N3	117.38(12)
O1–Fe–N1	139.55(12)

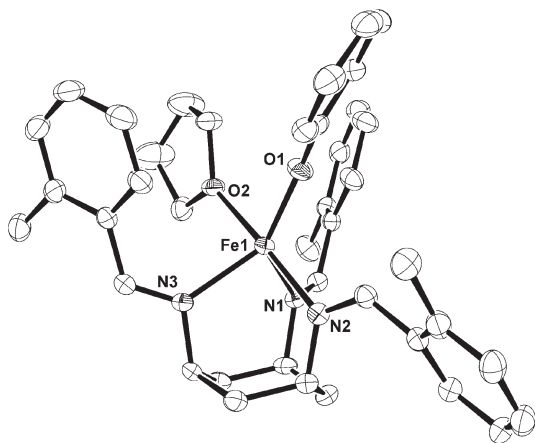


**Figure 8.** Solid state structure of [Fe(*cis*-TACH-*o*-tolyl)(phenolate)](THF)OTf (**7**) with ellipsoids shown at 50% probability. Hydrogen atoms and triflate anion are omitted for clarity.

Using the deconvolution function of TopSpin,<sup>24</sup> it was possible to calculate the integrations of the overlapped signals to be roughly 2:1 for each set of split peaks.

These data can be interpreted through the following model. At room temperature, all three tolylidene arms are equivalent, because the phenolate can sample the space

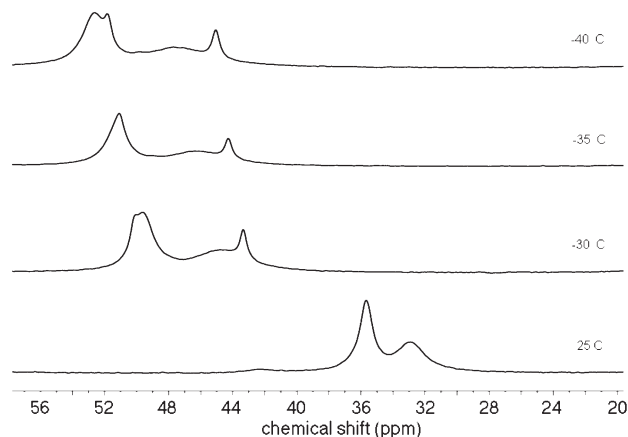


**Figure 9.** Low-temperature <sup>1</sup>H NMR spectra of the solution resulting from the mixture of iron(II) triflate, **1**, and sodium 2,6-dichlorophenolate in CD<sub>3</sub>CN, showing the signals for the cyclohexane β protons of the TACH-*o*-tolyl ligand. The lowest temperature (decoalesced) spectrum is at the top. The change in chemical shifts arises from the usual temperature dependence of the hyperfine shifts expected for an *S* = 2 complex. The full spectra are shown in the Supporting Information.

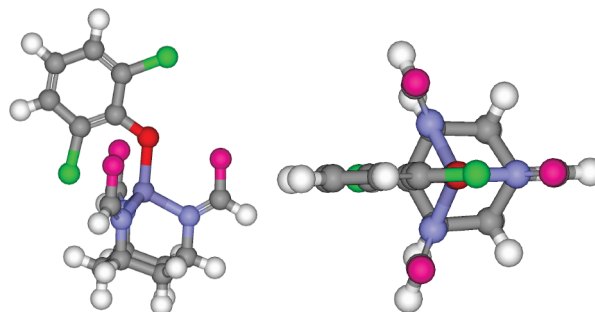


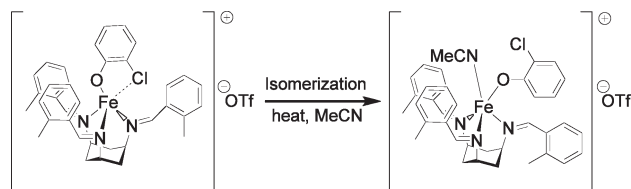
**Figure 10.** Two views of a proposed solution structure of **2**, shown without tolyl groups for clarity. A mirror plane containing the phenolate and bisecting the cyclohexyl ring is responsible for two different cyclohexane β proton environments, and it explains the decoalescence of the two <sup>1</sup>H NMR signals between δ 30 and 40 ppm and the 2:1 integration pattern of the decoalesced signals.

between each set of tolylidene arms. At low temperature, this motion around the Fe–O bond is slowed, and the phenolate is trapped between a single set of ligand arms (as found in the crystal structure) on the NMR time scale. Without rotation around the iron–oxygen bond, there is only one plane of symmetry, which runs through the metal center and bisects the cyclohexane ring of the TACH ligand (Figure 10). This causes there to be two inequivalent types of cyclohexane ring β protons, leading to low-temperature splitting into the observed 2:1 integration pattern. Note, however, that there is no evidence for decoalescence of the phenolate *meta* proton signals. Therefore, the rotation of the phenolate O–C bond in solution remains rapid on the NMR time scale down to –40 °C, in contrast to the crystal structures, where a single phenolate orientation is observed.

Other <sup>1</sup>H NMR studies examined the nature of the isomerization of the imine N=C bonds in the tolylidene arms. The [Fe(*cis*-TACH-*o*-tolyl)(2-chlorophenolate)]OTf complex (**4**) was analyzed by <sup>1</sup>H NMR spectroscopy and compared to the spectrum of **3** in CD<sub>3</sub>CN, discussed above. Since **4** has one *cis*-imine arm and two *trans*-imine arms, it no longer has *C*<sub>3</sub> symmetry, and is predicted to

(24) Topspin, 1.3; Bruker: Rheinstetten, Germany, 2005.



**Scheme 3.** Isomerization of the TACH-*o*-tolyl Ligand

have at most  $C_s$  symmetry. Consistent with this lower-symmetry point group, the  $^1\text{H}$  NMR spectrum of **4** contains more signals than the spectrum of **3** (see Supporting Information). The imine protons and the cyclohexane  $\alpha$ -CH are no longer all equivalent, and instead of two highly downfield signals integrating to 3H each, there are four signals, two that integrate to 1H and two that integrate to 2H. This observation is consistent with the expected mirror plane of symmetry in the molecule. The remaining highly overlapped signals between  $\delta$  18 and  $-6$  ppm are not amenable to further characterization. The unique methyl group of the isomerized tolylidene is identified at  $\delta$   $-4.2$  ppm from its integration. In solution, the THF molecule bound to the metal in the solid state structure of **4** is presumably displaced by the more strongly donating  $\text{CD}_3\text{CN}$ , although the congestion of signals around  $\delta$  2 and 4 ppm in the  $^1\text{H}$  NMR spectrum precludes any attempt at assigning peaks to bound solvent. Without considering bound solvent, 21  $^1\text{H}$  NMR signals are expected and 20 distinct signals are observed. The approximate number of signals and the integration values of the non-overlapping peaks are consistent with the solid-state structure.

To further investigate the isomerization of TACH-*o*-tolyl, a  $\text{CD}_3\text{CN}$  solution containing **1**, iron(II) triflate and 2-chlorophenolate was heated at  $60^\circ\text{C}$ , and  $^1\text{H}$  NMR spectra were taken periodically. Initially, the spectrum corresponded to that of **3**. Over several hours,  $^1\text{H}$  NMR signals corresponding to **3** diminished in intensity while signals corresponding to **4** began to emerge, with a half-life of about an hour. Cooling the solution back to room temperature did not change the ratio of products by  $^1\text{H}$  NMR spectroscopy. Samples of **4** in  $\text{CD}_3\text{CN}$  did not convert to **3** even after several days in solution at room temperature. The thermal stability of **4** was confirmed by heating a sample in  $\text{CD}_3\text{CN}$  to  $65^\circ\text{C}$  for 10 min, but no changes were observed in the  $^1\text{H}$  NMR spectrum. Thus, the isomerization of the imine in one tolylidene arm is favorable and irreversible under these conditions (Scheme 3).

While the 2-chlorophenolate complex could be crystallized with the TACH-*o*-tolyl ligand in the desired all *trans* orientation as well as the *cis*-isomerized form, the unsubstituted phenolate complex was crystallized only with the tridentate ligand in the *cis*-isomerized form. Accordingly,  $^1\text{H}$  NMR studies (see Supporting Information) show that “Fe(TACH-*o*-tolyl)(phenolate)”, which displays the  $C_3$  symmetry indicative of the all *trans* ligand geometry, converts in 3 h at  $60^\circ\text{C}$  to the isomerized ligand complex, **7**, which has  $C_s$  symmetry. The signals corresponding to  $(\text{TACH-}o\text{-tolyl})\text{Fe}(\text{OTf})_2$  and  $\text{Fe}(\text{phenolate})_x$  remain unchanged.

## Discussion

**Tridentate Imine Ligands Based on TACH.** We report here the first examples of iron(II) complexed to a triimine that is based on the triaminocyclohexane (TACH) core.

Hexadentate, trianionic TACH-based ligands have been coordinated to iron(III) to form neutral, coordinatively saturated complexes.<sup>16c,25</sup> Though **1** is a new TACH-based ligand, it is closely related to mesityl and benzyl substituted ligands that have been complexed to Cu and Ni.<sup>17,19</sup> To date, the only examples of an iron(II) complex bound to a TACH-based ligand use the parent triaminocyclohexane.<sup>26</sup>

One persistent problem that plagued the studies reported here was that TACH-*o*-tolyl could be displaced by strong donors. For example, addition of excess phenolate caused loss of the tridentate ligand. To explain this observation, note that the favored conformation of the free triimine has all three substituents in equatorial positions. To coordinate to a metal, these substituents must reach axial positions. Therefore, despite the advantages of the chelate effect, there is an unfavorable enthalpic contribution to metal binding by this tridentate ligand.

One advantage to the TACH-based triimine ligands is that the ligand synthesis gives imines that each have a *trans* stereochemistry. Upon metal coordination, *trans* imine substituents are constrained to form “walls” around the remaining binding sites, which restrict the number of additional ligands. The crystal structures of **2**, **3**, and **6** show that the imine substituents surround the fourth donor to the iron(II) center, and prevent phenolates from bridging to a second metal. Variable-temperature  $^1\text{H}$  NMR studies suggest that in **2**, the movement of the fourth ligand around the binding site is restricted. We assume that Fe–O bond rotation is somewhat hindered in complexes **3** and **6** as well, though we could not reach temperatures low enough to cause decoalescence of peaks in their  $^1\text{H}$  NMR spectra. Overall, TACH-imine ligands are excellent at sterically protecting the phenolate binding site, and give mononuclear, high-spin iron(II) complexes.

However, certain difficulties are present because the *trans*-imines are thermodynamically disfavored in the metal complexes. Walton and co-workers have reported the hydrolysis of the imine  $\text{C}=\text{N}$  bonds in benzyldiene substituted TACH type ligands;<sup>17</sup> however in the work reported here, hydrolysis was prevented by the stringent exclusion of water. Although we were able to circumvent hydrolysis as a problem with TACH-imine based complexes, we uncovered another problem: imine isomerization. As evidenced by the solid-state structures of **4**, **5**, and **7**, one tolylidene arm of the TACH-*o*-tolyl ligand can isomerize from *trans* to *cis*. Monitoring the transformation to these species by  $^1\text{H}$  NMR spectroscopy showed that the isomerization of imines from *trans* to *cis* is thermodynamically favored. Control studies showed that **1** isomerizes only in the presence of metal. We are not aware of previous examples in the literature of arm isomerization in transition-metal complexes of TACH-imine ligands. Qualitative measurements showed that *ortho*-substituents on the phenolate slowed the arm isomerization.

**Synthesis of Iron(II) Phenolate Complexes with a Bulky Supporting Ligand.** Though the coordination of phenolate-like species to non-heme iron(II) complexes is important

(25) (a) Bollinger, J. E.; Mague, J. T.; Oconnor, C. J.; Banks, W. A.; Roundhill, D. M. *J. Chem. Soc., Dalton Trans.* **1995**, 1677–1688. (b) Bollinger, J. E.; Mague, J. T.; Roundhill, D. M. *Inorg. Chem.* **1994**, *33*, 1241–1242.

(26) Yang, J. Y.; Shores, M. P.; Sokol, J. J.; Long, J. R. *Inorg. Chem.* **2003**, *42*, 1403–1419.

for understanding enzymes that process these aromatics, the coordination chemistry of high-spin, non-heme iron(II) complexes with phenolates has primarily used phenolates that are tethered as part of a multidentate ligand.<sup>27</sup>

Iron(II) complexes with unsupported phenolates are much less common, and require ligands that constrain the iron coordination sphere. The most common supporting ligands are based on porphyrin.<sup>28</sup> Phenoxide has been attached to a [4Fe-4S] cluster in the  $\text{Fe}_2^{2+}\text{Fe}_2^{3+}$  state.<sup>29</sup> Dinuclear complexes have been reported with 2,4,6-tri-*t*-butylphenolate as a bridging ligand and as both a bridging and terminal ligand.<sup>30</sup> A series of four-coordinate tris(pyrazolyl)borate-supported iron(II) phenolate complexes were characterized by <sup>1</sup>H NMR, IR, MCD, and elemental analysis.<sup>31,32</sup> A crystal structure was reported for one of these, with pentafluorophenolate.<sup>27</sup> The known chemistry of halogenated phenolates on iron(II) is even more scarce. To our knowledge there are no iron(II) 2-chlorophenolate or 2,6-dibromophenolate complexes reported in the literature. Iron(II) complexes coordinated with 2,6-dichlorophenolate have been reported, but not characterized fully.<sup>31,32</sup> No crystallized iron 2-methylphenolate complexes have been reported in the literature, and only iron(III) 2-methylphenolate complexes have been reported thus far.<sup>33</sup> Thus, there is a lack of information in the literature regarding the behavior of halogenated phenolates on iron(II) that could provide insight into the origin of substrate specificity in PcpA and LinE.

The work reported herein shows that the  $[\text{Fe}(\text{TACH-}o\text{-tolyl})]^{2+}$  system provides a platform for the synthesis of complexes with a variety of substituted phenolates. Though these complexes in some cases could not be purified to analytical purity, we have obtained <sup>1</sup>H NMR solution characterization for complexes with five different substituted phenolates as well as unsubstituted phenolate and 2-methylhydroquinonate. Crystal structures of four of the substituted phenolate complexes were obtained, with chloro-, bromo-, and methyl- substituents at the *ortho* positions. Each iron-containing cation is paired with an outer-sphere triflate, which was evident from the crystal structure as well as the characteristic bands in the infrared spectrum near 1263, 1154, and 1030  $\text{cm}^{-1}$ .<sup>34</sup> A crystal structure was also obtained for the unsubstituted phenolate complex, albeit with the tolylidene arm isomerized to the *cis*-orientation. The 2-methylhydroquinonate complex was unstable in solution and resisted all attempts at

crystallization. Nonetheless, since there are no mononuclear hydroquinone complexes with iron(II) in the literature, the solution characterization reported herein is an important first step in accumulating structural information on how substituted hydroquinone substrates may bind to the iron(II) center in the enzymes LinE and PcpA. In particular, the phenolate complexes provide critical insights into the role of the *ortho* substituent, as will be described below.

**Comparison of the Structures of the (TACH-*o*-tolyl)Fe(phenolate) Complexes.** The structures of the iron phenolate complexes fall into two distinct categories: (1) compounds **2**, **3**, **5**, and **6** have only the TACH-*o*-tolyl ligand and phenolate coordinated to the iron(II) center, and (2) compounds **4** and **7** that have an additional solvent molecule bound to the iron(II) center.

In complexes **2**, **3**, **5**, and **6**, the structure of the TACH-iron(II) unit is highly conserved. In the structures of the metal-TACH-imine ligands in the literature, the average  $\text{M}-\text{N}_{\text{imine}}$  bond distance is 2.06(7) Å, regardless of metal identity or TACH ligand substitution.<sup>16–19</sup> This is similar to the values observed in the TACH-*o*-tolyl iron(II) complexes reported here, where the average  $\text{Fe}-\text{N}$  bond distance of the *trans* TACH-*o*-tolyl complexes is 2.09(2) Å and the values range from 2.061 Å ( $\text{Fe}-\text{N3}$  in **2A**) to 2.143 Å ( $\text{Fe}-\text{N1}$  in **2B**), with  $\text{Fe}-\text{N1}$  being slightly longer than the other two distances in all of the structures but **6**. The three  $\text{N}-\text{Fe}-\text{N}$  angles are distinctly different in each structure. One of the  $\text{N}-\text{Fe}-\text{N}$  angles is always significantly larger than the other two, and in each case, these two nitrogen atoms hold the tolylidene arms that sandwich the phenolate ( $\text{N2}$  and  $\text{N3}$ ). This  $\text{N}-\text{Fe}-\text{N}$  angle ranges from 95.7° in **6** to 97.8° in **2A**. The other two  $\text{N}-\text{Fe}-\text{N}$  angles show somewhat more variability, and range from 83.1° (for  $\text{N3}'-\text{Fe}'-\text{N1}'$  in **3B**) to 97.1° (for  $\text{N3}-\text{Fe}-\text{N1}$  in **2B**). Overall, the  $\text{Fe}-\text{N}$  bond lengths and  $\text{N}-\text{Fe}-\text{N}$  angles in these complexes appear to be constrained by the rigidity of the cyclohexane ring, and many aspects of the geometry of the bound  $\text{Fe(II)}$  in these complexes are dictated by the core of the tridentate ligand.

In each of these four compounds (**2**, **3**, **5**, and **6**), there is a close interaction between the phenolate aromatic ring and two *o*-tolyl groups of the supporting TACH-*o*-tolyl ligand (minimum ring–ring distances of 3.2–3.5 Å). These are well within the distance usually accepted as  $\pi$ -stacking.<sup>35</sup> This observation raises the issue of whether the strength of  $\pi$ -stacking influences the binding of different phenolates. The nature of electronic effects on  $\pi$ -stacking has been the source of recent controversy: though the traditional view holds that electron-withdrawing substituents increase the strength of  $\pi$ -stacking interactions, gas-phase and computational studies have questioned the generality and trends in this interaction.<sup>36</sup> In the compounds described here, there is no compelling evidence for significant differences in  $\pi$ -stacking, because the shortest ring–ring distances are similar in the dichlorophenolate complex **2** as in the methylphenolate complex **6** (both 3.2 Å).

(35) Hunter, C. A.; Sanders, J. K. M. *J. Am. Chem. Soc.* **1990**, *112*, 5525–5534.

(36) A review of different viewpoints may be found in: Wheeler, S. E.; McNeil, A. J.; Müller, P.; Swager, T. M.; Houk, K. N. *J. Am. Chem. Soc.* **2010**, *132*, 3304–3311.

(27) There are more than 100 crystallographically characterized iron(II) complexes with tethered phenolates as part of supporting multidentate ligands, primarily derived from salen. Selected examples: (a) Jameson, G. B.; March, F. C.; Robinson, W. T.; Koon, S. S. *J. Chem. Soc., Dalton Trans.* **1978**, 185–191. (b) Cini, R. *Inorg. Chim. Acta* **1983**, *73*, 146–152. (c) Kayal, A.; Lee, S. C. *Inorg. Chem.* **2002**, *41*, 321–330; see also ref 21.

(28) (a) Ainscough, E. W.; Addison, A. W.; Dolphin, D.; James, B. R. *J. Am. Chem. Soc.* **1978**, *100*, 7585–7591. (b) Phillippi, M. A.; Shimomura, E. T.; Goff, H. M. *Inorg. Chem.* **1981**, *20*, 1322–1325.

(29) Weigel, J. A.; Holm, R. H. *J. Am. Chem. Soc.* **1991**, *113*, 4184–4191.

(30) Bartlett, R. A.; Ellison, J. J.; Power, P. P.; Shoner, S. C. *Inorg. Chem.* **1991**, *30*, 2888–2894.

(31) Ito, M.; Amagai, H.; Fukui, H.; Kitajima, N.; Moro-oka, Y. *Bull. Chem. Soc. Jpn.* **1996**, *69*, 1937–1945.

(32) Pavel, E. G.; Kitajima, N.; Solomon, E. I. *J. Am. Chem. Soc.* **1998**, *120*, 3949–3962.

(33) (a) Richard, M. J.; Shaffer, C. D.; Evilia, R. F. *Electrochim. Acta* **1982**, *27*, 979–983. (b) Arasasingham, R. D.; Balch, A. L.; Hart, R. L.; Latograzynski, L. J. *J. Am. Chem. Soc.* **1990**, *112*, 7566–7571.

(34) Johnston, D. H.; Shriver, D. F. *Inorg. Chem.* **1993**, *32*, 1045–1047.

In **4** and **7**, where one of the tolylidene arms has isomerized to the *cis* orientation, the iron(II) is trigonal bipyramidal with a THF bound between the two *trans* tolylidene ligand arms. The axial ligands in the trigonal bipyramid are the THF oxygen atom (O2) and the nitrogen atom from the isomerized imine (N2). The trigonal bipyramidal geometry is demonstrated by the nearly linear O2–Fe–N2 angles of 174.73(4)° in **4** and 174.74(8)° in **7**, and by the fact that N3, N1, and O1 compose a plane with the sum of their angles equaling 360.0(1)° in **4** and 359.7(2)° in **7**. Instead of stacking between the *trans* tolylidenes as seen in all of the structures that lack a bound solvent, the phenolate is bent into the open space created by the isomerized *cis*-tolylidene. Reducing steric congestion likely offsets the small energetic stabilization lost from the disruption of  $\pi$ -stacking found in the structures of the *trans*-TACH-*o*-tolyl complexes.

**Evidence for Secondary Bonding Interactions of Halogenated Phenolates with Iron(II).** LinE and PcpA are unique in their ability to cleave chlorinated hydroquinones. What drives this substrate selectivity is not well understood.<sup>9</sup> The basic coordination chemistry of halogenated phenols with iron(II) has been left unexplored in the literature. The complexes herein represent the first *ortho*-chlorophenolate-iron(II) complexes to be crystallographically characterized.<sup>37</sup> Compound **5** is the first example of an iron 2,6-dibromophenolate complex. Interestingly, our <sup>1</sup>H NMR studies indicate that *ortho*-halophenolates bind completely to TACH-ligand iron complexes while unsubstituted phenolate and 2-methylphenolate do not. These results suggest that the presence of a halogen adjacent to the hydroxyl group of a phenolate may stabilize its iron(II) complexes.

The increased stability of the iron(II) phenolate complexes with *ortho*-halogen substituents, combined with the structural evidence that shows the halogen substituents oriented toward the iron(II) center in all of the structures with all-*trans*-TACH ligands, suggests that an iron–halogen interaction may be important in these complexes. Electronic interactions between metals and the chlorine atoms of chloroarenes have been reported in the literature.<sup>38</sup> Wulfsberg and co-workers have postulated that when the distance between the metal (M) and the chlorine of the chloroarene is within 1.0 Å of the average M–chloride distance for that metal, a secondary

**Table 6.** Comparison between Fe–Halogen Distances in TACH-*o*-tolyl-iron(II) Complexes Reported Here<sup>a</sup>

[Fe(TACH- <i>o</i> -tolyl)( <u>    </u> )] <sup>+</sup> OTf <sup>–</sup>	Fe–halogen distance (Å)	$\Delta$ average Fe–halogen (Å)
2-chlorophenolate	2.929(7)	0.72(6)
	3.010(8)	0.80(6)
2,6-dichlorophenolate A	3.122(2)	0.91(6)
2,6-dichlorophenolate B	2.890(2)	0.68(6)
2,6-dichlorophenolate C	2.988(2)	0.78(6)
2,6-dibromophenolate	2.8414(3)	0.49(4)

<sup>a</sup> These may be compared to the average Fe–halogen bond length in the Cambridge Structural Database (2.21(6) Å for Fe–Cl and 2.35(4) Å for Fe–Br).<sup>40</sup> The second column gives the difference between the Fe–halogen distance in the TACH-*o*-tolyl supported complexes and the average Fe–halogen bond length.

bonding interaction is likely.<sup>39</sup> Table 6 compares the Fe–Cl(chloroarene) distances of the TACH-*o*-tolyl-Fe(II) complexes to the average Fe–Cl(chloride) bond length for four-coordinate iron(II) chloride complexes of 2.21 Å (standard deviation 0.06 Å).<sup>40</sup> The TACH-*o*-tolyl supported iron-phenolate complexes exhibit Fe–Cl distances ranging from 2.890(2) to 3.122(2) Å, and therefore they meet Wulfsberg's criterion for a secondary interaction. The evidence for secondary interactions between iron and the bromine substituent in the 2,6-dibromophenolate complex is even more convincing, with a Fe–Br distance less than 0.5 Å longer than the average from the Cambridge Structural Database (2.35 Å; standard deviation 0.04 Å). Previous workers have seen that the strength of secondary interactions increases with heavier halogen atoms.<sup>38d</sup> There is only one reported example of an *ortho*-bromophenolate complex that exhibits a metal–halogen secondary bond.<sup>41</sup>

There are other structural differences between halogenated (**2**, **3**, **5**) and non-halogenated (**6**) phenolate complexes. For example, there are significant differences in the Fe–O(aryl) distance among the different complexes. The Fe–O1 distances vary from 1.865(3) to 1.915(7) Å for complexes **2**, **3**, and **5**, while non-halogenated **6** has the shortest distance at 1.858(3) Å. This is suggestive of a lower coordination number in the absence of the iron–halogen interaction. Additionally, the N1–Fe–O1 angles for complexes **2**, **3**, and **5** vary from 100.29(5)° to 127.84°, while the angle in **6** is anomalous at 139.55(12)°. This difference can also be attributed to an iron–halogen interaction that constrains the Fe–O–C angle.

It is also possible to show that the tetrahedral geometry of the methyl-substituted compound **6** is distorted toward a trigonal bipyramid in **2**, **3**, and **5**. There are two ways to probe the extent to which the geometry of the Fe–N2–N3–O1 unit is trigonalized. First, for a trigonal (bi)pyramidal geometry, atoms N2, N3, and O1 compose a plane, and the sum of the N2, N3, and O1 angles about the iron(II) center should be 360°. This sum is 358.9(2)° in the 2,6-dibromophenolate complex **5**, making it the most trigonal.

(40) Our values come from a search of terminal Fe-halide complexes with four-coordinate iron, from structures without disorder, with *R* < 10%, in the Cambridge Crystallographic Database (November 2009). Similar numbers are quoted in the literature: Orpen, A. G.; Brammer, L.; Allen, F. H.; Kennard, O.; Watson, D. G.; Taylor, R. *J. Chem. Soc., Dalton Trans.* **1989**, S1–S83.

(41) Camurlu, P.; Yilmaz, A.; Tatar, L.; Kisakürek, D.; Ülkü, D. *Cryst. Res. Technol.* **2005**, *40*, 271–276.

(37) There are two crystallographically characterized iron(III) phenolate compounds with 2,6-chloro substituents. (a) Koch, S. A.; Millar, M. *J. Am. Chem. Soc.* **1982**, *104*, 5255–5257. (b) Helms, A. M.; Jones, W. D.; McLendon, G. L. *J. Coord. Chem.* **1991**, *23*, 351–359.

(38) Examples: (a) Meyer, R.; Gagliardi, J.; Wulfsberg, G. *J. Mol. Struct.* **1983**, *111*, 311–316. (b) Wulfsberg, G.; Yanisch, J.; Meyer, R.; Bowers, J.; Essig, M. *Inorg. Chem.* **1984**, *23*, 715–719. (c) Colman, M. R.; Newbound, T. D.; Marshall, L. J.; Noirot, M. D.; Miller, M. M.; Wulfsberg, G. P.; Frye, J. S.; Anderson, O. P.; Strauss, S. H. *J. Am. Chem. Soc.* **1990**, *112*, 2349–2362. (d) Kulawiec, R. J.; Crabtree, R. H. *Coord. Chem. Rev.* **1990**, *99*, 89–115. (e) Garcia, M. P.; Jimenez, M. V.; Cuesta, A.; Siurana, C.; Oro, L. A.; Lahoz, F. J.; Lopez, J. A.; Catalan, M. P.; Tiripicchio, A.; Lanfranchi, M. *Organometallics* **1997**, *16*, 1026–1036. (f) Poignant, G.; Nlate, S.; Guerchais, V.; Edwards, A. J.; Raithby, P. R. *Organometallics* **1997**, *16*, 124–132. (g) Wulfsberg, G.; Parks, K. D.; Rutherford, R.; Jackson, D. J.; Jones, F. E.; Derrick, D.; Ilsley, W.; Strauss, S. H.; Miller, S. M.; Anderson, O. P.; Babushkina, T. A.; Gushchin, S. I.; Kravchenko, E. A.; Morgunov, V. G. *Inorg. Chem.* **2002**, *41*, 2032–2040.

(39) Richardson, M. F.; Wulfsberg, G.; Marlow, R.; Zaghonni, S.; McCorkle, D.; Shadid, K.; Gagliardi, J.; Farris, B. *Inorg. Chem.* **1993**, *32*, 1913–1919.



This sum is somewhat smaller for the 2-chloro- and 2,6-dichlorophenolate complexes, ranging from  $339.0(3)^\circ$  to  $356(1)^\circ$ , while in methylphenolate complex **6** this sum is much smaller at  $325.4(2)^\circ$ . The second measure of deviation from a perfect trigonal (bi)pyramidal geometry is the N3–Fe–N2–O1 torsion angle. A value of  $180^\circ$  indicates that O1 lies directly in the same plane as the N3–Fe–N2 unit. The N3–Fe–N2–O1 torsion angle of **5** is the closest to the ideal value at  $169.8(1)^\circ$ . This torsion angle is somewhat smaller in the 2-chloro- and 2,6-dichlorophenolate complexes, ranging from  $134.4(3)^\circ$  to  $160(1)^\circ$ . In contrast, the N3–Fe–N2–O1 torsion angle for **6** is only  $122.7(2)^\circ$ . Thus, the halogen-substituted complexes are more trigonal than the 2-methylphenolate complex, suggesting that the halogen influences the geometry at iron(II), distorting the tetrahedral geometry toward a five-coordinate trigonal bipyramidal geometry in which one of the five bonds to the iron(II) center is a secondary bonding interaction with the halogen. This is shown clearly in Figure 11, where the cyclohexyl rings of complexes **2**, **3**, **5**, and **6** have been overlaid. The *ortho*-halogen atoms of the phenolates in **2**, **3**, and **5** are similarly placed, while the 2-methylphenolate lies drastically out of the N2, N3, O1 plane.

The 2,6-dibromophenolate complex **5** is the most trigonal bipyramidal of the halophenolate complexes. For example, the N1–Fe–Br angle in **5** is closest to linear at  $174.99(3)^\circ$ . The N1–Fe–Cl angles in the 2,6-dichloro- and 2-chlorophenolate complexes are somewhat smaller, ranging from  $163.4(5)^\circ$  to  $168.5(5)^\circ$ . Another measure is the  $\tau_5$  value, where a  $\tau_5$  value of 1.0 represents a perfect trigonal bipyramidal geometry and 0.0 represents a square pyramidal geometry.<sup>42</sup> The  $\tau_5$  values of these complexes range from 0.408(3) for **2C** to 0.617(1) for **5**. (These values are somewhat less than 1.0 because of the constraints of the chelating ligand, which prevent the complex from achieving perfect  $90^\circ/120^\circ$  angles.)

Thus, comparison of the structures of **2**, **3**, **5** versus **6** illustrates that *ortho*-halogen substitution on the phenolate ring alters the placement of the phenolate. The proximity of the halogen to the metal center and its location as one of the positions in a trigonal bipyramidal geometry are consistent with a halogen-iron interaction. The different orientation of the *ortho*-substituent in the 2-methylphenolate complex (**6**)—despite the similar steric demands of a methyl versus a chloro-substituent—suggest that an iron–halogen interaction is responsible for the halogen orientation and the coordination geometry in **2**, **3**, and **5** rather than sterics or crystal packing. The shorter distance of the Fe–halogen interaction and the closer agreement to trigonal bipyramidal geometry in the 2,6-dibromophenolate complex (**5**) compared to any of the structures of 2-chloro- and 2,6-dichlorophenolate complexes are particularly noteworthy. This difference may indicate that secondary bond formation to an iron(II) is especially favorable for softer Lewis bases such as bromine substituents.

Although secondary iron–halogen interactions most coherently explain the trends seen in this work, it is important to consider other possible reasons for the observed trend of halogenated phenolates binding more strongly to the iron

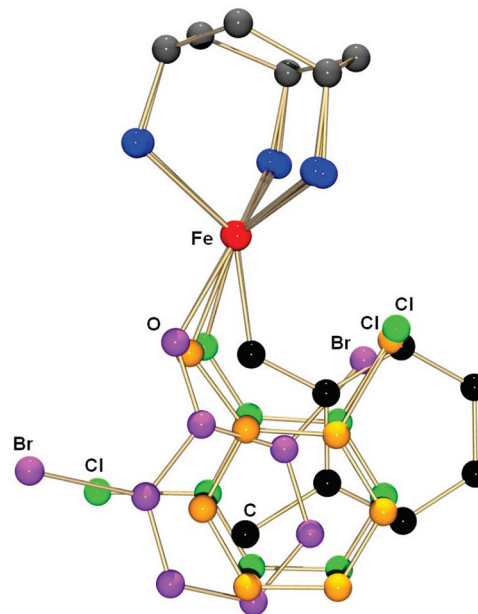


**Figure 11.** Comparison of the solid-state structures of 2,6-dichlorophenolate **2B** (green), 2-chlorophenolate **3A** (orange), 2,6-dibromophenolate **5** (purple), and 2-methylphenolate **6** (black). The TACH rings are overlaid, and tolylidene arms are removed for clarity. This shows that the halogen substituent undergoing the secondary bonding interaction is always in nearly the same position, and also that the 2-methylphenolate complex **6** (in black) has a significantly different conformation than the *ortho*-halogenated phenolates.

atom than the non-halogenated phenolates. First, one could envision  $\pi$ -bonding between the phenolate oxygen lone pairs and half-filled d orbitals on the iron ion. However, iron-to-oxygen  $\pi$ -donation would be expected to be greatest with electron-donating phenolate substituents, and in our study electron-withdrawing phenolates were bound most strongly. On the other hand, electron-withdrawing substituents are known to increase the strength of polar M–X  $\sigma$ -bonds by stabilizing the partial negative charge on X.<sup>43</sup> Thus, this effect might play a role in the trend observed here. Second,  $\pi$ -stacking between TACH-*o*-tolyl aromatic groups and the phenolates is present and could contribute. However, as mentioned above, the ring–ring distances are similar for all complexes of the *trans*-TACH-*o*-tolyl ligand, suggesting that differences in  $\pi$ -stacking strength are minimal. Naturally, we cannot rule out energetic influences on  $\pi$ -stacking that do not significantly influence the structures. Third, differences in the enthalpies of solvation of the different phenolates provides another possible contribution to the binding enthalpies; however, the solvation enthalpies are not known for the halogenated phenolates studied here. Each of these differences (secondary bonding, the strength of the Fe–O bond,  $\pi$ -stacking, and solvation) would have to be considered to provide a complete account of the thermodynamic differences between the binding of phenolates with and without *ortho*-halogen substituents.

**Biological Relevance.** The active site structure of PcpA has not been crystallographically determined; however,

(42) Addison, A. W.; Rao, T. N.; Reedijk, J.; Vanrijn, J.; Verschoor, G. C. *J. Chem. Soc., Dalton Trans.* **1984**, 1349–1356.

(43) (a) Erikson, T. K. G.; Bryan, J. C.; Mayer, J. M. *Organometallics* **1988**, 7, 1930–1938. (b) Holland, P. L. *Comments Inorg. Chem.* **1999**, 21, 115–129.

site-directed mutagenesis and homology modeling indicate that the iron(II) ion is ligated to two histidines and a glutamate as in EDOs.<sup>9</sup> In the model complexes, these biological metal donors are mimicked by a symmetric tris-imine ligand. Though the electronic properties are certainly not identical between the chelating ligand used here and the biological donor set, the TACH-based ligand benefits from *o*-tolyl substituents that protect the binding pocket, preventing bridging phenolates and giving a mononuclear iron(II) complex with a geometry that should be considered as possible in the enzyme–substrate adduct. The most significant result in the studies reported here is that a close iron–halogen contact is present, and contributes to the strength of phenolate binding. This suggests that the chlorinated hydroquinones that are oxidatively cleaved by the hydroquinone dioxygenases could bind to the non-heme iron(II) site of the enzyme through a weak interaction with the *ortho* chlorine of the substrate with the metal. Because the substrate of hydroquinone dioxygenases has only one coordinating oxygen atom, there is a site on the iron(II) for this secondary interaction, whereas the two coordinating oxygen atoms in the extradiol catechol dioxygenase enzymes do not leave space for an interaction between the metal ion and the halogen substituents. We suggest that in PcpA and LinE, the weak iron–chlorine interaction may orient the hydroquinone in the binding pocket for productive cleavage and provide tighter binding of the substrate to the enzyme.

## Conclusions

The new ligand TACH-*o*-tolyl can be synthesized in high yields, and it forms a 1:1 ligand:metal complex with iron(II). When combined with iron(II) triflate and substituted phenolates, TACH-*o*-tolyl forms 1:1:1 ligand:iron:phenolate complexes, which have been characterized both in the solid state and in solution. Despite being tridentate, the neutral ligand is labile when complexed with iron(II) and phenolate. When heated to moderate temperatures, a tolylidene arm in the 1:1:1 iron:TACH-*o*-tolyl:phenolate complexes can isomerize from *trans* to *cis* geometry, increasing the size of the binding pocket at the metal. In the isomerized complexes, the metal can bind a solvent molecule, while in the all *trans* ligand complexes, there is no coordinated solvent.

The complexes containing TACH-*o*-tolyl with *ortho*-halo-substituted phenolates exhibit Fe–halogen distances that are short enough to qualify as secondary bonding interactions. The geometries of these complexes also reflect the interaction between the iron and halogen and are best described as trigonal bipyramidal, while the complex containing a non-coordinating *ortho*-methyl substituent is four-coordinate. Further, the *ortho*-methyl group is pointed away from the metal, despite the similar steric demands of the methyl and chloro substituents. In solution, only phenolates with *ortho*-halo substituents yielded complete binding to the complex, suggesting that a metal–halogen interaction stabilizes the complexes as well. The iron(II)–halogen secondary bond in these complexes may point toward an explanation for the substrate specificity of PcpA and LinE, enzymes whose function is to oxidatively cleave chlorinated substrates. In these enzymes, a metal–chlorine interaction may improve substrate binding and orient the substrate in the active site

to promote chemoselective and regioselective C–C bond cleavage.

## Experimental Section

**General Considerations.** All manipulations were carried out under an N<sub>2</sub> atmosphere using standard Schlenk techniques or in an M. Braun glovebox maintained at or below 1.0 ppm of O<sub>2</sub>. Acetonitrile, pentane, dichloromethane, diethyl ether, and THF were dried using activated alumina and “deoxygenizer” columns from Glass Contour Co. (Laguna Beach, CA) prior to use. Glassware was dried at 150 °C overnight. Celite was dried at 200 °C under vacuum prior to use.

Deuterated acetonitrile was degassed using the freeze–pump–thaw method and then dried over 4 Å molecular sieves three successive times. Deuterated THF and dimethoxyethane were dried over CaH<sub>2</sub>, then over sodium metal and then vacuum distilled into a storage container before use. NMR spectra in CD<sub>3</sub>CN, CD<sub>2</sub>Cl<sub>2</sub>, and C<sub>4</sub>D<sub>8</sub>O (Cambridge Isotopes) were recorded using a Bruker Avance 400 (400 MHz) and Bruker Avance 500 (500 MHz) instruments. Acquisition parameters were designed to suppress diamagnetic signals with long relaxation times, whereas signals from high-spin iron complexes have relaxation times < 10 ms. Typical parameters: acquisition time = 132 ms; preacquisition delay time = 4.5 μs; delay time = 400 ms; pulse width = 3.15 μs; sweep width = 3.0 × 10<sup>5</sup> Hz; number of scans = 64. All peaks are singlets unless otherwise specified. Frequencies were referenced to the signal of CD<sub>2</sub>HClN at δ 1.94 ppm, CDHCl<sub>2</sub> at δ 5.32 ppm, and C<sub>4</sub>D<sub>7</sub>HO at δ 3.58 and 1.73 ppm. <sup>19</sup>F NMR spectra were referenced to an external standard of hexafluorobenzene at δ –164.9 ppm.

Electronic spectra (shown in Supporting Information) were recorded from 200 to 700 nm on a Cary 50 UV–visible spectrophotometer using quartz cuvettes of 1 cm optical path length. Air sensitive electrospray mass spectrometry used a gastight Hamilton syringe and direct injection of dilute solution samples into the electrospray chamber of an Agilent LC/MS. IR spectra of anhydrous KBr pellets and solid samples were recorded on a Shimadzu 8400S FT-IR spectrometer. Elemental analyses were determined at the microanalysis facilities at the University of Illinois, Urbana–Champaign or at the University of Rochester.

Reagents, unless otherwise noted, were purchased from Aldrich or Alfa Aesar and used without purification. All phenols were sublimed under vacuum or, if liquid, distilled, degassed, and stored over fresh 4 Å sieves prior to use. 2-Methylhydroquinone was crystallized from dry Et<sub>2</sub>O and dried under vacuum. It was essential that all phenols and hydroquinones be purified and dried. Iron(II) triflate was used as its bis-acetonitrile adduct, and was prepared according to a literature method.<sup>44</sup> For synthesis of phenolate complexes for X-ray crystallographic studies, the sublimed, dried phenols were generally treated with one molar equivalent of triethylamine to generate [HNEt<sub>3</sub>][phenolate] solutions in either THF (more often) or acetonitrile (in a few cases). In these reactions, the use of highly purified THF (freshly passed through activated alumina, even after drying and degassing through standard techniques) was essential for the effective synthesis of iron(II) complexes.

**Synthesis of *cis,cis*-1,3,5-Tris-(*E*)-(ortho-tolyldeneimino)cyclohexane (TACH-*o*-tolyl (1)).** **Method 1.** Potassium hydroxide (157 mg, 2.90 mmol) was dissolved in H<sub>2</sub>O (1 mL) and added to TACH·3HBr (315 mg, 0.850 mmol). The solution was stirred until the TACH salt dissolved producing a colorless solution. *Ortho*-tolualdehyde (0.300 mL, 2.45 mmol) was added to diethyl ether (2.5 mL), and the mixture was added to the rapidly stirring aqueous solution. The biphasic mixture was stirred rapidly overnight, resulting in a white solid. H<sub>2</sub>O (10 mL) was added

(44) Hagadorn, J. R.; Que, L.; Tolman, W. B. *Inorg. Chem.* **2000**, *39*, 6086–6090.



to the reaction mixture, and the product was extracted with chloroform ( $3 \times 20$  mL). The combined organic layers were washed with  $\text{H}_2\text{O}$  ( $2 \times 10$  mL), dried with  $\text{Na}_2\text{SO}_4$ , filtered, and solvent was removed in vacuo for at least 6 h to yield a white powder (300 mg, 0.69 mmol, 81%). The product may be further purified by crystallization under  $\text{N}_2$  from hot, anhydrous acetonitrile (12 mL) yielding a colorless microcrystalline solid (260 mg, 0.597 mmol, 70%). Attaining analytical purity required subsequent washing with an aqueous EDTA solution, perhaps removing small amounts of adventitious  $\text{Zn(II)}$ .  $^1\text{H}$  NMR (400 MHz,  $\text{CDCl}_3$ ):  $\delta$  8.69 (s, 3H, HC=N), 7.87 (d, 3H, *o*-ArH,  $J = 7.6$  Hz), 7.62 (m, 6H, two ArH), 7.16 (d, 3H, ArH,  $J = 7.2$  Hz), 3.60 (m, 3H, cyclohexyl), 2.50 (s, 9H,  $\text{CH}_3$ ), 2.13 (dd, 3H, cyclohexyl,  $J = 23$  Hz,  $J = 12$  Hz), 1.93 (m, 3H, cyclohexyl).  $^{13}\text{C}\{^1\text{H}\}$  NMR (500 MHz,  $\text{CDCl}_3$ ):  $\delta$  158.1 (C=N), 137.6 (Ar), 134.6 (Ar), 130.8 (Ar), 130.2 (Ar), 127.8 (Ar), 126.3 (Ar), 67.0 (cyclohexyl), 41.4 (cyclohexyl), 19.5 ( $\text{CH}_3$ ). IR (solid sample): 1632 (s), 1599 (w), 1575 (w), 1483 (w), 1458 (w), 1440 (w), 1387 (w), 1376 (w), 1343 (w), 1285 (w), 1220 (w), 1156 (w), 1120 (w), 1086 (w), 1016 (w), 973 (w), 951 (w), 940 (w), 873 (w), 857 (w), 754 (s), 746 (s), 716 (m), 696 (w), 667 (w), 636 (w), 575 (w)  $\text{cm}^{-1}$ . Elem. Anal. Calcd: C, 82.72; H, 7.64; N, 9.65. Found: C, 82.78; H, 7.67; N, 9.70.

**Method 2.** This procedure is adapted from the literature.<sup>19</sup> Toluene (25 mL) was added to TACH-3HBr (535 mg, 1.44 mmol) in a round-bottom flask followed by *ortho*-tolualdehyde (0.500 mL, 4.32 mmol) and triethylamine (0.600 mL, 4.32 mmol). The reaction was refluxed for 18 h using a Dean–Stark trap to remove water by azeotropic distillation. The solution was allowed to cool to room temperature, water (25 mL) was added to the solution, and the product was extracted with chloroform ( $3 \times 25$  mL). The combined organics were dried with  $\text{Na}_2\text{SO}_4$ , filtered, and solvent removed under reduced pressure for at least 6 h to yield a white powder (460 mg, 1.06 mmol, 78%). The material could be further purified by washing the solid with  $\text{Et}_2\text{O}$ , dissolving in hot, dry acetonitrile, and cooling to room temperature to precipitate. The product was spectroscopically identical to that from Method 1.

**[Fe(TACH-*o*-tolyl)(2,6-dichlorophenolate)]OTf (2).**  $\text{Fe}(\text{OTf})_2 \cdot 2\text{CH}_3\text{CN}$  (45 mg, 0.10 mmol) was dissolved in  $\text{CH}_3\text{CN}$  (4 mL) and added to **1** (44 mg, 0.10 mmol). Sodium 2,6-dichlorophenolate (19 mg, 0.10 mmol) was dissolved in  $\text{CH}_3\text{CN}$  (4 mL) and added to the solution containing iron and ligand. The solution immediately turned brilliant yellow and was stirred for 2 h. The sample was concentrated to 4 mL, filtered through Celite, and all solvent was removed in vacuo. The solid was washed with diethyl ether (7 mL) and dried under vacuum yielding a bright yellow powder (77 mg, 0.096 mmol, 96%). Judging from  $^1\text{H}$  NMR spectroscopy, the yellow powder contains some of the *cis*-TACH-*o*-tolyl complex. To separate isomers, crystallization is necessary. Crystals suitable for analysis by X-ray diffraction were obtained from vapor diffusion of  $\text{Et}_2\text{O}$  into a concentrated THF solution at  $-35^\circ\text{C}$ .  $^1\text{H}$  NMR (500 MHz,  $\text{CD}_3\text{CN}$ ):  $\delta$  308 (3H, imine H or cyclohexane  $\alpha\text{C-H}$ ), 292 (3H, imine H or cyclohexane  $\alpha\text{C-H}$ ), 61.6 (2H, *m*-phenolate H), 35.8 (3H, cyclohexane  $\beta\text{C-H}$ ), 33.0 (3H, cyclohexane  $\beta\text{C-H}$ ), 11.2 (3H, tolyl H), 9.1 (3H, tolyl H), 7.3 (3H, tolyl H),  $-12.3$  (9H, tolyl Me),  $-28.9$  (1H, *p*-phenolate H),  $-47.7$  (3H, tolyl H) ppm. IR (KBr): 3063 (w), 2924 (w, br), 2860 (w), 1621 (m), 1598 (m), 1462 (s), 1442 (w), 1309 (m), 1266 (s), 1223 (s), 1154 (m), 1119 (w), 1031 (m), 873 (w). UV–vis: see Supporting Information. ES-MS:  $m/z = 652.10$   $[\text{M}]^+$ , (calcd 652.16). Elem. Anal. Calcd: C, 55.38; H, 4.52; N, 5.24. Found: C, 55.03; H, 4.48; N, 5.28.

**[Fe(TACH-*o*-tolyl)(2-chlorophenolate)]OTf (3).**  $\text{Fe}(\text{OTf})_2 \cdot 2\text{CH}_3\text{CN}$  (43 mg, 0.099 mmol) was dissolved in  $\text{CH}_3\text{CN}$  (3 mL) and added to **1** (43 mg, 0.099 mmol). Sodium 2-chlorophenolate (15 mg, 0.099 mmol) was dissolved in acetonitrile (2 mL) and added to the ligand-iron solution. The bright yellow solution was stirred for 30 min, and concentrated to less than 0.5 mL. Addition of  $\text{Et}_2\text{O}$  (2 mL) caused precipitation of a yellow, microcrystalline solid. After decanting the supernatant, the

yellow solid was washed with  $\text{Et}_2\text{O}$  (5 mL) and dried under vacuum (43.1 mg, 0.059 mmol, 60%). Single crystals suitable for analysis by X-ray diffraction were obtained from vapor diffusion of  $\text{Et}_2\text{O}$  into a concentrated THF solution at  $-35^\circ\text{C}$ .  $^1\text{H}$  NMR (500 MHz,  $\text{CD}_3\text{CN}$ ):  $\delta$  308 (3H, imine H or cyclohexane  $\alpha\text{C-H}$ ), 290 (3H, imine H or cyclohexane  $\alpha\text{C-H}$ ), 67.7 (1H, *m*-phenolate H), 59.8 (1H, *m*-phenolate H), 37.6 (3H, cyclohexane  $\beta\text{C-H}$ ), 34.6 (3H, cyclohexane  $\beta\text{C-H}$ ), 11.6 (1H, *o*-phenolate), 10.7 (3H, tolyl H), 7.2 (3H, tolyl H), 3.1 (3H, tolyl H),  $-13.0$  (9H, tolyl Me),  $-29.5$  (1H, *p*-phenolate),  $-42.2$  (3H, tolyl H) ppm. UV–vis: see Supporting Information. As this complex readily isomerizes, see  $[\text{Fe}(\text{cis-TACH-}o\text{-tolyl})(2\text{-chlorophenolate})(\text{THF})]^+ \text{OTf}^-$  (**4**) for additional characterization.

**[Fe(*cis*-TACH-*o*-tolyl)(2-chlorophenolate)(THF)]OTf (4).**  $\text{Fe}(\text{OTf})_2 \cdot 2\text{CH}_3\text{CN}$  (45 mg, 0.10 mmol) was dissolved in  $\text{CH}_3\text{CN}$  (4 mL) and added to **1** (45 mg, 0.10 mmol). Sodium 2-chlorophenolate (16 mg, 0.10 mmol) was dissolved in  $\text{CH}_3\text{CN}$  (4 mL) and added to the TACH-ligand iron solution. The bright yellow solution was stirred overnight. The solution was filtered through Celite and concentrated to less than 1 mL. Diethyl ether (3 mL) was added resulting in a white precipitate, and the yellow solution was filtered and solvent removed in vacuo. The yellow-orange oil was extracted with  $\text{Et}_2\text{O}$  ( $2 \times 10$  mL) leaving behind a white powder. The  $\text{Et}_2\text{O}$  washes were combined, and  $\text{Et}_2\text{O}$  was removed under vacuum resulting in a yellow-orange powder (64 mg, 0.070 mmol, 70%).  $\text{Et}_2\text{O}$  vapor diffusion into a concentrated THF solution gave X-ray quality crystals (44 mg, 0.052 mmol, 52%). As discussed in the text, the  $^1\text{H}$  NMR spectrum contains regions of extreme signal congestion, therefore signal assignments and integrations are not all specified.  $^1\text{H}$  NMR (500 MHz,  $\text{CD}_3\text{CN}$ ):  $\delta$  260 (2H, imine H or cyclohexane  $\alpha\text{-CH}$ ), 253 (1H, imine H or cyclohexane  $\alpha\text{-CH}$ ), 243 (2H, imine H or cyclohexane  $\alpha\text{-CH}$ ), 239 (1H, imine H or cyclohexane  $\alpha\text{-CH}$ ), 54.8, 51.4, 50.62, 15.7 (2H), 10.2, 9.00, 8.25, 6.06 (1H), 5.09 (1H), 4.20, 3.66, 1.13, 0.98,  $-1.37$  (6H, Me),  $-4.17$  (3H, Me),  $-28.3$  (2H) ppm. IR (KBr): 3055 (w), 2974 (m, br), 2935 (m, br), 2890 (m, br), 1620 (m), 1600 (m), 1580 (m), 1477 (s), 1463 (m), 1439 (m), 1426 (w), 1385 (w), 1316 (s), 1265 (s), 1224 (s), 1160 (s), 1121 (m), 1030 (s), 983 (w), 944 (w), 866 (m). ES-MS:  $m/z = 618.10$   $[\text{M}]^+$ , (calcd 690.25, loss of THF = 618.20). Elem. Anal. Calcd: C, 58.61; H, 5.40; N, 5.00. Found: C, 57.11; H, 5.35; N, 4.69. The disagreement indicates that small amounts of impurities are present.

**[Fe(*cis*-TACH-*o*-tolyl)(2,6-dibromophenolate)]OTf (5).**  $\text{Fe}(\text{OTf})_2 \cdot 2\text{CH}_3\text{CN}$  (98.2 mg, 0.225 mmol) was dissolved in  $\text{CH}_3\text{CN}$  (6 mL) and added to **1** (98.2 mg, 0.225 mmol). 2,6-Dibromophenol (56.7 mg, 0.225 mmol) was dissolved in  $\text{CH}_3\text{CN}$  (17 mL) and  $\text{Et}_3\text{N}$  (31  $\mu\text{L}$ , 0.22 mmol) was added to the solution. Addition of the 2,6-dibromophenolate solution to the iron solution resulted in an immediate bright orange colored solution, and the solution was stirred for 90 min. The solution was filtered and solvent removed in vacuo. The orange solid was dissolved in DME (2 mL), and yellow crystals were obtained through diffusion of  $\text{Et}_2\text{O}$  at room temperature overnight (138 mg, 0.154 mmol, 69%).  $^1\text{H}$  NMR (500 MHz,  $\text{CD}_3\text{CN}$ ) for initial complex before isomerization to the *cis* form:  $\delta$  292 (3H, imine H or cyclohexane  $\alpha\text{C-H}$ ), 286 (3H, imine H or cyclohexane  $\alpha\text{C-H}$ ), 60.2 (2H, *m*-phenolate H), 31.4 (3H, cyclohexane  $\beta\text{C-H}$ ), 29.2 (3H, cyclohexane  $\beta\text{C-H}$ ), 10.5 (3H, tolyl H), 9.3 (3H, tolyl H), 7.5 (3H, tolyl H),  $-11.0$  (9H, tolyl Me),  $-30.3$  (1H, *p*-phenolate H),  $-41$  (3H, tolyl H) ppm. IR (KBr): 3057 (w), 3018 (w), 2976 (w), 2959 (w), 2934 (m), 2916 (m), 1612 (s), 1568 (m), 1454 (s), 1423 (s), 1260 (vs), 1152 (s), 1119 (m), 1031 (s), 867 (s), 851 (m), 775 (m), 748 (s), 716 (s), 636 (s), 573 (w). UV–vis: see Supporting Information. Elem. Anal. Calcd: C, 49.85; H, 4.07; N, 4.71. Found: C, 49.63; H, 3.88; N, 4.52.

**[Fe(TACH-*o*-tolyl)(2-methylphenolate)]OTf (6).**  $\text{Fe}(\text{OTf})_2 \cdot 2\text{CH}_3\text{CN}$  (108 mg, 0.25 mmol) was dissolved in  $\text{CH}_3\text{CN}$  (6 mL)



Table 7. Crystal and Data Parameters for the X-ray Crystal Structures of 2–7

	2A	2B, 2C	3	4	5	6	7
empirical formula	C <sub>37</sub> H <sub>36</sub> Cl <sub>2</sub> F <sub>3</sub> Fe N <sub>3</sub> O <sub>4</sub> S	C <sub>37</sub> H <sub>36</sub> Cl <sub>2</sub> F <sub>3</sub> Fe N <sub>3</sub> O <sub>4</sub> S	C <sub>37</sub> H <sub>37</sub> Cl F <sub>3</sub> Fe N <sub>3</sub> O <sub>4</sub> S	C <sub>49</sub> H <sub>61</sub> Cl F <sub>3</sub> Fe N <sub>3</sub> O <sub>7</sub> S	C <sub>37</sub> H <sub>36</sub> Br <sub>2</sub> F <sub>3</sub> Fe N <sub>3</sub> O <sub>4</sub> S	C <sub>38</sub> H <sub>40</sub> F <sub>3</sub> Fe N <sub>3</sub> O <sub>4</sub> S	C <sub>45</sub> H <sub>56</sub> F <sub>3</sub> Fe N <sub>3</sub> O <sub>6</sub> S
formula weight	802.50	802.50	768.06	984.37	891.42	747.64	879.84
temperature (K)	100.0(1)	100.0(1)	100.0(1)	100.0(1)	100.0(1)	100.0(1)	100.0(1)
wavelength (Å)	0.71073	0.71073	0.71073	0.71073	0.71073	0.71073	0.71073
crystal system	monoclinic	orthorhombic	monoclinic	triclinic	triclinic	monoclinic	monoclinic
space group	<i>P</i> 2 <sub>1</sub> / <i>c</i>	<i>P</i> 2 <sub>1</sub> 2 <sub>1</sub> 2 <sub>1</sub>	<i>P</i> 2 <sub>1</sub> / <i>n</i>	<i>P</i> $\bar{1}$	<i>P</i> $\bar{1}$	<i>P</i> 2 <sub>1</sub> / <i>c</i>	<i>P</i> 2 <sub>1</sub> / <i>n</i>
<i>a</i> (Å)	14.686(4)	14.6868(15)	16.9571(17)	10.2579(6) Å	10.6512(11)	12.5196(15)	15.789(5)
<i>b</i> (Å)	16.131(4)	16.0815(16)	11.3491(11)	11.6864(7)	12.1541(12)	18.836(2)	11.047(3)
<i>c</i> (Å)	15.192(4)	32.540(3)	19.949(2)	20.0868(13)	15.2230(15)	15.5583(19)	25.260(8)
$\alpha$ (deg)	90	90	90	81.558(1)	92.183(2)	90	90
$\beta$ (deg)	101.686(5)	90	112.264(2)	84.955(1)	97.622(2)	108.099(2)	94.905(5)
$\gamma$ (deg)	90	90	90	84.044(1)	112.503(2) <sup>o</sup>	90	90
volume (Å <sup>3</sup> )	3524.5(16)	7685.5(13)	3552.9(6)	2362.5(3)	1796.1(3)	3487.4(7)	4390(2)
<i>Z</i>	4	8	4	2	2	4	4
crystal color, morphology	yellow, plate	yellow-orange, plate	yellow, plate	yellow-orange, block	yellow, block	orange, needle	yellow-orange, needle
crystal size (mm)	0.26 × 0.22 × 0.04	0.26 × 0.20 × 0.04	0.26 × 0.20 × 0.08	0.36 × 0.30 × 0.26	0.22 × 0.18 × 0.12	0.16 × 0.06 × 0.04	0.36 × 0.16 × 0.05
data/restraints/parameters	6232/0/463	15710/19/996	6290/127/625	20481/16/512	17055/0/463	7131/0/455	11784/6/550
GOF on <i>F</i> <sup>2</sup>	0.963	0.995	1.043	1.005	1.022	0.984	1.009
final <i>R</i> indices [ <i>I</i> > 2σ( <i>I</i> )]	<i>R</i> 1 = 0.0514 <i>wR</i> 2 = 0.0985	<i>R</i> 1 = 0.0586 <i>wR</i> 2 = 0.0787	<i>R</i> 1 = 0.0702 <i>wR</i> 2 = 0.1842	<i>R</i> 1 = 0.0461 <i>wR</i> 2 = 0.1176	<i>R</i> 1 = 0.0359 <i>wR</i> 2 = 0.0812	<i>R</i> 1 = 0.0582 <i>wR</i> 2 = 0.0897	<i>R</i> 1 = 0.0578 <i>wR</i> 2 = 0.1353
<i>R</i> indices (all data)	<i>R</i> 1 = 0.1394 <i>wR</i> 2 = 0.1394	<i>R</i> 1 = 0.1228 <i>wR</i> 2 = 0.0979	<i>R</i> 1 = 0.1336 <i>wR</i> 2 = 0.2328	<i>R</i> 1 = 0.0629 <i>wR</i> 2 = 0.1247	<i>R</i> 1 = 0.0565 <i>wR</i> 2 = 0.0879	<i>R</i> 1 = 0.1376 <i>wR</i> 2 = 0.1120	<i>R</i> 1 = 0.1116 <i>wR</i> 2 = 0.1583

and added to **1** (108 mg, 0.25 mmol). 2-Methylphenol (27 mg, 0.25 mmol) was dissolved in CH<sub>3</sub>CN (6 mL) and Et<sub>3</sub>N (35 μL, 0.25 mmol) was added to the solution. Addition of the 2-methylphenolate solution to the iron solution resulted in an immediate bright orange colored solution, and the solution was stirred for 30 min. The solution was filtered and solvent removed in vacuo. The orange solid was dissolved in DME (2 mL), and orange crystals were obtained through diffusion of Et<sub>2</sub>O at room temperature overnight (two crops, 90 mg, 0.18 mmol, 72%). <sup>1</sup>H NMR (500 MHz, CD<sub>3</sub>CN): δ 299 (3H, imine H or cyclohexane αC–H), 283 (3H, imine H or cyclohexane αC–H), 76.7 (3H, 2-methylphenolate CH<sub>3</sub>), 62.7 (1H, *m*-phenolate H), 57.2 (1H, *m*-phenolate H), 28.9 (3H, cyclohexane βC–H), 26.8 (3H, cyclohexane βC–H), 26.0 (1H, *o*-phenolate H), 11.8 (3H, tolyl H), 8.8 (3H, tolyl H), 7.1 (3H, tolyl H), –9.7 (9H, tolyl Me), –23.0 (3H, tolyl H), –39.3 (1H, *p*-phenolate H) ppm. IR (KBr): 3062 (w), 3039 (w), 3008 (w), 2948 (w), 2922 (w), 2895 (w), 1618 (m), 1597 (m), 1484 (m), 1455 (w), 1444 (w), 1426 (w), 1401 (w), 1265 (s), 1250 (s), 1169 (m), 1148 (m), 1124 (w), 1085 (w), 1064 (w), 1043 (m), 1031 (s), 872 (w), 858 (w), 750 (m), 715 (w). Elem. Anal. Calcd: C, 60.96; H, 5.52; N, 5.61. Found: C, 60.07; H, 5.25; N, 5.74.

[Fe(*cis*-TACH-*o*-tolyl)(phenolate)(THF)]<sup>+</sup> OTf<sup>–</sup> (**7**). Fe(OTf)<sub>2</sub>·2CH<sub>3</sub>CN (36 mg, 0.084 mmol) was dissolved in CH<sub>3</sub>CN (7 mL) and added to **1** (37 mg, 0.085 mmol). Sodium phenolate (9.8 mg, 0.084 mmol) was dissolved in CH<sub>3</sub>CN (4 mL) and the solution added to the TACH-ligand iron solution. The bright yellow solution was stirred for 1.5 h and then concentrated to 2 mL. Diethyl ether (5 mL) was added resulting in white precipitate that was removed by filtering over Celite. Solvent was removed in vacuo leaving a yellow powder. The yellow colored compound was extracted from the solid by washing with Et<sub>2</sub>O (2 × 7 mL). Solvent was removed from the combined Et<sub>2</sub>O washes resulting in a yellow-orange powder (42 mg, 0.057 mmol, 68%). There are small amounts of *trans*-TACH-*o*-tolyl iron-phenolate complex in the product. Heating drives the mixture completely to the *cis* isomer. Crystals suitable for X-ray diffraction were obtained from a concentrated solution of THF/Et<sub>2</sub>O, made by heating, with Et<sub>2</sub>O vapor diffusion at –35 °C. As discussed in the text, the <sup>1</sup>H NMR spectrum contains many overlapping signals, therefore not all signal assignments and integrations can be specified.

<sup>1</sup>H NMR of [Fe(*cis*-TACH-*o*-tolyl)(phenolate)(CH<sub>3</sub>CN)]<sup>+</sup> OTf<sup>–</sup> (500 MHz, CD<sub>3</sub>CN): δ 252 (2 signals, 1H + 2H, imine H or cyclohexane α-CH), 242 (1H, imine H or cyclohexane α-CH), 237 (2H, imine H or cyclohexane α-CH), 54.7, 52.0 (2 signals, 1H + 2H, phenolate), 39.0 (1H, phenolate), 32.5 (1H), 13.1, 10.4, 8.70, 8.29, 7.78, 7.19, 5.96, 4.46, 3.59, 2.45, –0.30, –3.40, –5.10, –15.1 (2H), –27.5 (1H), –30.43 (2H, phenolate) ppm. IR (KBr): 3063 (w), 3022 (w), 2925 (w), 2885 (w), 1621 (m), 1593 (m), 1587 (m), 1487 (m), 1458 (w), 1443 (w), 1423 (w), 1385 (w), 1266 (s), 1154 (m), 1121 (w), 1031 (m), 922 (w), 919 (w), 860 (m), 755 (s), 695 (w). UV–vis: see Supporting Information. ES-MS: *m/z* = 584.15 [M]<sup>+</sup>, (calcd 656.29, loss of THF = 584.24) Elem. Anal. Calcd: C, 61.12; H, 5.75; N, 5.22. Found: C, 59.97; H, 5.99; N, 5.04. The disagreement indicates that small amounts of impurities are present.

If the reagents are mixed and the <sup>1</sup>H NMR spectrum is collected quickly before isomerization, [Fe(TACH-*o*-tolyl)(phenolate)]<sup>+</sup> OTf<sup>–</sup> can be observed. <sup>1</sup>H NMR of [Fe(TACH-*o*-tolyl)(phenolate)]<sup>+</sup> OTf<sup>–</sup> (500 MHz, CD<sub>3</sub>CN): δ 279 (3H, imine H or cyclohexane α-CH), 265 (3H, imine H or cyclohexane α-CH), 58.7 (2H, *m*-phenolate), 38.9 (2H, *o*-phenolate), 20.6 (2 overlapping signals), –12.3 (9H, tolyl Me), –36.9 (1H, *p*-phenolate) ppm, diamagnetic region overlaps with free TACH-*o*-tolyl and Fe(TACH-*o*-tolyl)(OTf)<sub>2</sub>.

**X-ray Crystallography.** Each crystal was placed onto the tip of a glass fiber and mounted on a Bruker SMART Platform diffractometer equipped with an APEX II CCD area detector. All data were collected at 100.0(1) K using MoKα radiation (graphite monochromator). For each sample a preliminary set of cell constants and an orientation matrix were determined from reflections harvested from three orthogonal wedges of reciprocal space. Full data collections were carried out with frame exposure times of 25–120 s at detector distances of 4 or 5 cm. Randomly oriented regions of reciprocal space were surveyed for each sample: three or four major sections of frames were collected with 0.50–1.00° steps in  $\omega$  at different  $\phi$  settings and detector positions of –33 or –38° in 2θ. The intensity data were corrected for absorption,<sup>45</sup> and final cell constants were

(45) Sheldrick, G. M. *SADABS*, version 2008/1; University of Göttingen: Göttingen, Germany, 2008.

calculated from the xyz centroids of approximately 4000 strong reflections from the actual data collection after integration.<sup>46</sup> Structures were solved using SIR97<sup>47</sup> and refined using SHELXL-97.<sup>48</sup> Direct-methods solutions were calculated which provided most non-hydrogen atoms from the difference Fourier map. Least squares (on  $F^2$ )/difference Fourier cycles located the remaining non-hydrogen atoms. Non-hydrogen atoms were refined with anisotropic displacement parameters, and hydrogen atoms were placed in ideal positions and refined as riding

(46) SAINT, version 7.60A; Bruker AXS: Madison, WI, 2008.

(47) Altomare, A.; Burla, M.; Cascarano, G. L.; Giacovazzo, C.; Guagliardi, A.; Moliterni, A. G. G.; Polidori, G.; Spagna, R. *SIR97: A new program for solving and refining crystal structures*; Istituto di Cristallografia, CNR: Bari, Italy, 1999.

(48) Allen, F. H. *Acta Crystallogr.* **2002**, *B58*, 380–388.

atoms with relative isotropic displacement parameters. Details of each structure are given in Table 7.

**Acknowledgment.** This research was supported by grants from the American Chemical Society–Petroleum Research Fund (ACS-PRF 44410-G3 to T.E.M.) and the National Science Foundation (CHE-0951999 to T.E.M. and CHE-0911314 to P.L.H.). Analytical data from the University of Rochester used the CENTC Elemental Analysis Facility, funded by NSF CHE-0650456.

**Supporting Information Available:** Crystallographic data is given in CIF format; further experimental details are given in Figures S1–S7. This material is available free of charge via the Internet at <http://pubs.acs.org>.